Diploma Thesis

Experimental investigation of the flow in a model of a blood vessel with an inserted flow obstacle

submitted in satisfaction of the requirements for the degree of

Diplom-Ingenieur

of the TU Wien, Faculty of Mechanical and Industrial Engineering

---

Diplomarbeit

Experimentelle Untersuchung der Strömung in einem Modell eines Blutgefäßes mit einem eingesetzten Strömungshindernis

ausgeführt zum Zwecke der Erlangung des akademischen Grades einer

Diplom-Ingenieurin

eingereicht an der Technischen Universität Wien, Fakultät für Maschinenwesen und Betriebswissenschaften

by

Lisa Huber, BSc

Matr.Nr.: 11775757

under the supervision of

Univ.Prof. Dipl.-Ing. Dr.techn. **Margit Gföhler**

Institute of Engineering Design and Product Development, E 307
Technische Universität Wien
Getreidemarkt 9, 1060 Wien, Österreich

Wien, April 11, 2023

Affidavit

I declare in lieu of oath, that I wrote this thesis and performed the associated research myself, using only literature cited in this volume. If text passages from sources are used literally, they are marked as such.

I confirm that this work is original and has not been submitted elsewhere for any examination, nor is it currently under consideration for a thesis elsewhere.

I acknowledge that the submitted work will be checked electrically-technically using suitable and state-of-the-art means (plagiarism detection software). On the one hand, this ensures that the submitted work was prepared according to the high-quality standards within the applicable rules to ensure good scientific practice "Code of Conduct" at the TU Wien. ON the other hand, a comparison with other student theses avoids violations of my personal copyright.

City and Date

Signature

Acknowledgements

I would like to express gratitude and thank to everybody who helped me during my master programm and during this master thesis.

Especially my supervisor, Margit Gföhler, to give me the opportunity to work on this project and realise my ideas.

Theresia Baumgartner for the endless hours in the PIV lab and the support when the printer was not working.

All the lovely and helpful people, working at the TU Wien, who helped me, by answering my questions or with their ideas.

My family for supporting me in every way during my master program.

All my friends, who let me talk their ears off when something was not working. Or took the time to drink a coffee with me and helped me bring my mind off the problems.

List of Abbreviations and Symbols

- $2D$ - 2 dimensional
- $3D$ - 3 dimensional
- BMS - Bare-Metal Stent
- cm - centimeter
- CAD - Computer Aided Design
- $CERAD$ - Covered Endovascular Reconstruction Of The Aortic Bifurcation
- $CVDs$ - Cardiovascular Diseases
- ΔT - delta T
- $DAPT$ - Dual Anti-Platelet Therapy
- DES - Drug-Eluting Stents
- FOV - Field Of View
- LDL - Low-Density Lipoprotein
- $HPIV$ - Holographic PIV
- H_2O - Water
- μm - micro meter
- mL/min - milliliter per minute
- mm - millimeter
- mm/s - millimeter per second
- $nd-YAG$ - neodym-yttrium aluminium garent
- PIV - Particle Image Velocimetry
- RI - Refractive Index

- ROI - Region Of Interest
- TE - Tunica Externa
- TI - Tunica Intima
- TM - Tunica Media
- UV - Ultraviolet
- WHO - World Health Organization

Abstract

Motivations The importance of stent implantation increases, due to the number of vascular diseases. But they also bear the risk of secondary thromboses. Therefore, a method was implemented to investigate the flow in blood vessels with a particle image velocimetry (PIV). The data from the 3D set-up specify the region of interest for the micro PIV experiments.

Methods Micro channels and the cylinder where designed in a way, that they would fit into the PIV system and match the requirements. The parts were printed with the Formlabs 2 printer and clear resin. Additionally, a post processing was done to the cylinders for the 3D measurements to increase the transparency. The attempt of designing a mold for a silicon form was made to create a dummy to mimic the blood vessel walls even further.

Results The 3D results show a lower velocity near the walls of the cylinder, which was expected. The micro channels too have a lower velocity near the walls and it changes with the design of the obstacles near the wall. A difference size of dead space was observed for different flow directions.

Zusammenfassung

Motivation Die Bedeutung der Stent-Implantation nimmt durch die Zahl der Gefäßerkrankungen zu, es besteht aber auch das Risiko von Folgethrombosen. Daher wurde eine Methode implementiert, um die Strömung in Blutgefäßen mit einer Particle Image Velocimetry (PIV) zu untersuchen. Die Daten aus dem 3D-Aufbau spezifizieren den Interessenbereich für die Mikro-PIV-Experimente.

Methoden Mikrokanäle und Zylinder wurden so konstruiert, dass sie in das PIV-System passen und den Anforderungen entsprechen. Die Teile wurden mit dem Formlabs 2-Drucker und transparentem Harz gedruckt. Zusätzlich wurden die Zylinder für die 3D-Messungen nachbearbeitet, um die Transparenz zu erhöhen. Der Versuch, eine Form für eine Silikonform zu entwerfen, wurde unternommen, um einen Dummy zu schaffen, der die Wände der Blutgefäße noch weiter nachahmt.

Resultate Die 3D-Ergebnisse zeigen, wie erwartet, eine niedrigere Geschwindigkeit in der Nähe der Zylinderwände. Auch die Mikrokanäle haben in Wandnähe eine geringere Geschwindigkeit, welche sich mit dem Design der Hindernisse ändert. Zusätzlich verändert die Strömungsrichtung die Größe des Totraumes um die Geometrie.

Contents

1 Introduction

According to the World Health Organization (WHO) the worlds population is getting older and most people will reach an age over 60. The number, of people over the age of 60, will double to 2.1 billion, compared to the 1.4 billion today. But with a longer life span also comes the health problems. To ensure a happy life at a higher age, personal health is the key factor - both mental and physical health.[1]

The most common negative health influences are hearing loss, osteoarthritis, pulmonary and cardiovascular diseases. [1] [2] Especially Cardiovascular diseases (CVDs) are one of the leading causes for deaths. Where stroke and heart attack are leading with 85 % of all deaths due to CVDs. They can be caused by narrowing the blood vessel or by clogging it with a blood clot. [2] The treatment for patients with this blockages are stents. Stents help to keep the vessel open and ensure a good blood supply. One of the main and most severe complications occurring during this treatment is secondary thrombosis due to flow issues in the blood vessel. [3] [4]

In this thesis, the goal is to detect and observe the influence different obstacles have on the flow and the problems faced when a stent is implemented. Additionally, to get a better understanding on the flow behavior shortly after the insertion of a stent and after the stent has been integrated into the vessel wall. Therefore, models representing a blood vessel with an inserted stent-like obstacle will be made. This model will show different geometries and the flow behavior will be studied with a particle imaging velocimetry system (PIV). The task for the 3D PIV is to find materials and geometries for the setup. Therefore, cylinders will be printed with a 3D printer and silicon mold will be manufactured. They will have a helix like structure to disturb the flow. Furthermore, for the μPIV channels with different geometries will be printed with the same 3D printer. The 3D PIV is used to locate areas with slow flow, which can be investigated on a more detailed level with a μPIV system. The flow behavior during the ingrowth of the

stent into the vessel wall will be simulated with three different circle shapes. The influence of different tilted obstacles will also be investigated. This should bring a better understanding on the influence different shapes will have on the blood flow and to therefore help to prevent problems due to dead space of slow flow.

It is expected, that channels with larger obstacles will have a larger dead space, before and after the geometries.

2 Theoretical background

In this chapter all necessary background information will be discussed. Starting with the anatomical structure of the blood vessel system, the risk given by thrombosis, the importance and the different designs of stents. Afterwards the functional principle of the PIV will be explained. The last part includes the selection of the used materials in this thesis.

2.1 Anatomical Structure Of The Blood Circulation System

The human body has a closed blood circulation system. It consists of a main pump - the heart - and bigger and smaller, pipe like, blood vessels. With this system oxygen, hormones, nutrients and other essential substances get transported through the whole body. [5]
The system is divided into the systemic circulation and the pulmonary circulation. In the systemic circulation, the blood gets transported through the body and is transporting the oxygen and nutrients. The bigger blood vessels get smaller until they cover the organs or spread in the limbs as a network of capillary vessels. The capillary system has a much thinner wall thickness than the bigger veins and arteries, therefore the oxygen exchange can take place. When the blood is pumped around the small or pulmonary circulation, the carbon dioxide - oxygen exchange between the surface of the lung and the capillary system takes place. [5]
In figure 2.1 this circulation systems is illustrated. The arrows are pointing in the direction of the blood flow while the color represents the amount of oxygen in the blood. The deoxygenated blood is pumped from the heart to the lung, where it is oxygenated. The oxygen rich blood flows back to the heart, which distributes it in the whole body. The cells exchange the oxygen with the carbon-dioxide, which leads back to the beginning of the cycle.

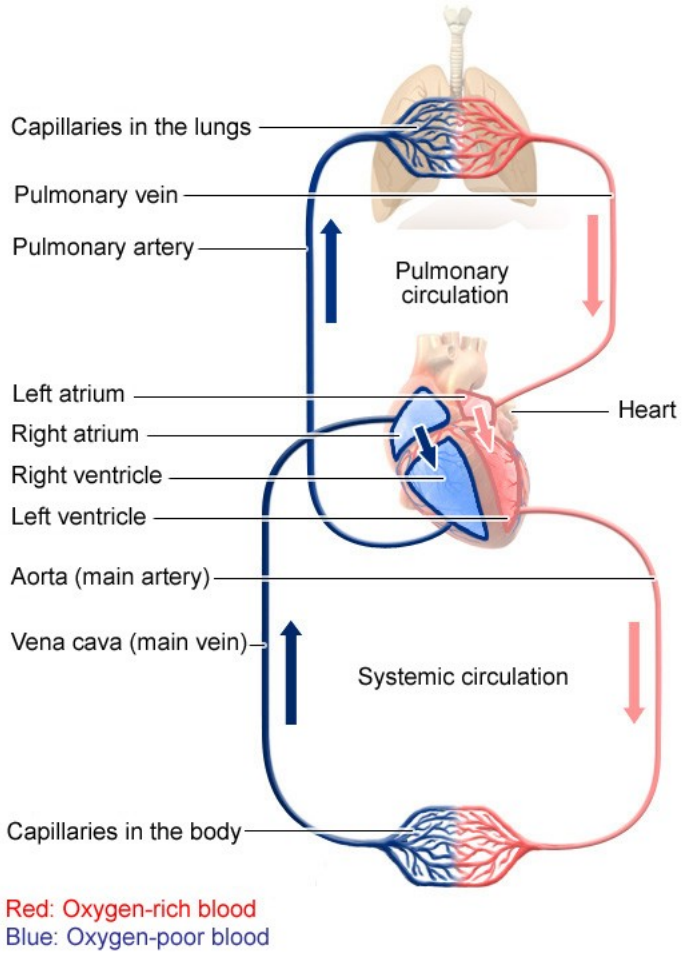

Figure 2.1: A systematic illustration of the blood vessel system of the human body. The two different colors represent the oxygen rich (red) and carbon dioxide rich (dark blue) state of the blood. The arrows show the direction of flow.[6]

2.1.1 Vessel-Wall Structure

The three main layers are the tunica intima (TI), which consists of endothelial cells, the tunica media (TM), composed of smooth muscle cells, elastin, collagen and proteoglycan, and the tunica externa (TE), building a collagen and elastin mesh, which conduce as a link layer between vessels and there surrounding. [7] [8]

Arteries overall, but in particular the Aorta, have to withstand high pressure. Therefore, they have a thick layer of TM, which can withstand pulsation and strain. The boundaries between the layers are distinct. The TI shows small collagen elastic fibers in flow direction. The fibers

from the TE are in longitudinal direction. The biggest vessel has a diameter of 3 cm. When arteries get smaller, mainly the TM gets decreased. The smallest vessels, before the capillaries, only have one muscle layer and a diameter of 20 - 80 μm. [7] [8]

Veins do not have sharp boundaries between the different layers. The TI can also show smooth muscle cells. The TM is thin and is sometimes separated into two layers. The thickest one is the TE, which also has muscle cells inside. As veins transport the blood back to the heart and often have to work against gravity, e.g. the legs, they have valves to stop the back flow of the blood. Veins range from 2 cm in diameter to 15 - 500 μm where they branch and merge with the capillaries. [7] [8]

Capillaries only consist of the TI, particularly linked endothelial cells. Some of the vessels are porous. The small diameter of 3 - 15 μm and the thickness of 0.1 - 1 μm enhance the gas exchange. [7] [8]

2.1.2 Pressure And Velocity Inside The Vessels

The pressure and velocity in the blood vessel system show many different values. The flux is pulsatile due to the mechanism of the heart. Therefore, the flow pattern differs a lot from the typical parabolic form, typical in tubes with a linear flux. The distribution of the blood vessels, into many branches, additionally prevent a formation of a parabolic flow pattern. Another interesting component for the flow is the behaviour of blood. The fact, that blood is a heterogeneous non-Newtonian fluid, its viscosity is dependent on the flow rate. If the flow rate decreases, the shear stress also decreases, but the viscosity increases drastically. [7]
The pulsatile flux has the biggest impact on the aorta. The aorta wall has to withstand the pressure and therefore expands. The pressure then increases slightly until the vessels branch out into arterioles and stays on a lower level until the blood enters the left atrium. A similar behaviour can be observed for the flow rate. As the flow rate in the aorta is around 15 - 20 cm/s it decreases to 0.02 - 0.01cm/sin the capillaries. The flow rate is inversely proportional to the cross section. As the cross section of all vessels in parallel increases from aorta to arteries

to capillaries the flow rate decreases. When the cross section decreases when the blood flows from the capillaries into the venule onward to the veins the flow rate increases again. [7]

2.1.3 Blood Components and Function

Blood consists of a variety of different components, but the two main ones are plasma and blood cells. Blood cells can be divided between red and white blood cells and plates. [9] [8] [7] There are around 5 million red blood cells, 7,500 white blood cells and 300,000 plates in one drop of blood. [9]

Plasma

Plasma consist of 91.5 % water, around 7 % proteins and the small rest of 1.5 % are solutes which are not proteins. This composition gives the plasma its typical color, of a clear light-yellow fluid. The composition also influences the blood pressure, as the amount of protein can alter with the viscosity of the blood. [9] [8] [7]
The main function of the plasma is to distribute and transport salt, gases, end products of the metabolism (glucose, fatty acids, vitamins), by-products of the liver, which need to be transported to the kidneys, anti-bodies and toxins.[9] [8] [7]

Red Blood Cells

Red blood cells are also called erythrocytes. They are around 7 - 10 μm in diameter discs with a biconcave shape. Despite their size, they are able to pass through capillaries with a diameter of 3 μm, due to their shape elasticity. [7] They are formed in the bone marrow of cancellous bone. In the beginning they all show a lower amount of haemoglobin but a nuclei. As the cell gets more mature, the nuclei start to disappear until there is no nuclei left in the finished cell. On the other hand, the haemoglobin ratio gets larger and larger. The haemoglobin is the important part for the oxygen and carbon dioxide ratio in the body, as haemoglobin attracts oxygen and is used for the transport. [9]

White Blood Cells

The function of white blood cells, leukocytes, is mainly to help the body to defend itself against strange substances in the body. Therefore, the cells are divided into different cell groups. The to main cell groups are lymphocytes and phagocytes. Lymphocytes start and channel the immune response of the body, while phagocytes locate and eliminate the anti-genes or invading microorganism. Phagocytes are divided into monocytes and granulocytes, latter are subdivided into neutrophils, to kill bacteria, eosinophils, activated for parasites and allergens, and basophils. [9] [7]

Plates

Plates or thrombocytes are needed for clotting and therefore prevent too much blood loss after a trauma. There are two different ways the clotting can be initiated. When the damage is done to cells, it is called the extrinsic way. The damaged cells will release thromboplastin. The thromboplastin attracts plates and they gather around the wound. The intrinsic way on the other hand starts inside a blood vessel. If there is damage to the vessel wall, plates will stick to this area. When plasma proteins get reformed into thrombin, which than build fibrin fibers. The fibrin forms threads which trap blood cells inside. This results in a clotting. If the blood clot is formed inside a blood vessel it is called thrombus. Which can lead to strokes, infarction and embolism if washed trough the body and clogging a small blood vessel. [9] [7]

2.1.4 Vasoconstriction

Diseases and defects in the cellular wall of blood vessels are one of the main causes for death in America and Europe, mainly atherosclerosis and aortic aneurysm. [10]

Sclerosis Sclerosis describes the incorporation of different cell times, e.g. lipids and T-Cells, into the cell wall. This leads to a reduction of blood flow by thickening of the vessel, compare figure 2.2 . It is a complex process of a long time inflammation, the response of the cells and later the migration and accumulation. [11] A huge factor for inflammation is the low-density lipoprotein (LDL) cholesterol. [12] There are three main categories for this type of migration,

depending on the cell time. The *fatty streak*, consists primarily of lipids and macrophages. The *fibrofatty plaque*, combining macrophages with lipid droplets with smooth muscle cells. The *fibrous plaque* dominated by smooth muscle cells. [10] [13]

If the plaque has built a compact outer shell and is separated from the blood flow nothing else will happen. But if the fibrous cap gets damaged, it can get dangerous. The rupture stimulates the blood clotting, *complicated plaques*. The plates will form a thrombus and if it gets washed away by the blood flow, it could block a small blood vessel which further can lead to a heart attack or stroke. [13]

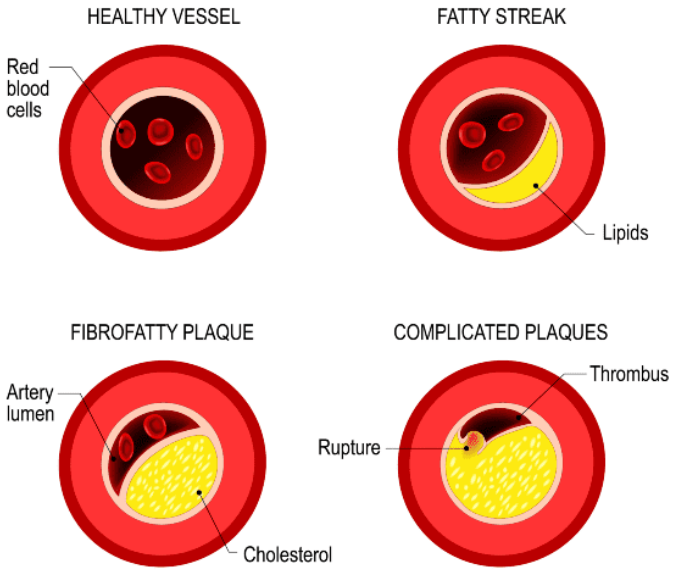

Figure 2.2: A healthy blood vessel and different types of sclerosis. [14]

Aneurysm In an aneurysm, the diameter of the blood vessel is extended. Aneurysms are most common in major vessels. Aneurysm can be categorized into true and false aneurysms.[15] The difference can be seen in figure 2.3, *(a)* represents a true aneurysm and *(b)* and *(c)* represent false aneurysms. True aneurysms are by definition responsible for an enlargement of the vessel diameter by at least 1.5 the time of the normal diameter. Additionally, all layers of the vessel wall are involved. If it bursts, it is in the early stage of formation. [16] False aneurysms on the other hand are more like a hematoma and appear when the vessel wall gets damaged. The aneurysms pulsate with every beating of the heart. The surrounding tissue also effects the speed with which the hematoma grows, until it ruptures. [17]

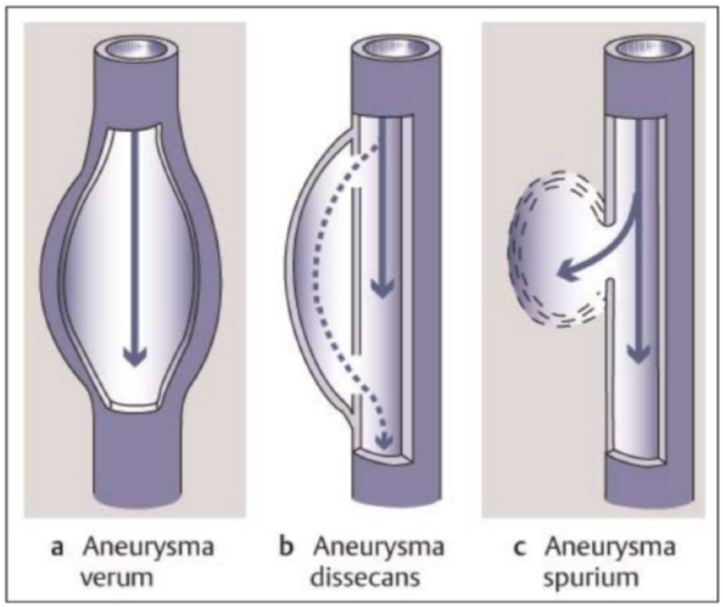

Figure 2.3: Different types of aneurysm. (a) is a true aneurysm, (b) and (c) are false aneurysms. [18]

2.2 Stent

The design of stents is a rather complex subject and will only be discussed briefly in this section.

Vascular surgery experienced a big change over the years, especially when stents were introduced. The development of stent crafts had to overcome a lot of obstacles before their performance was as good as today. But no patient is the same, so different blood vessel diseases need different treatments, either with medication or with surgery. [19] [20]

At the beginning of stents, they were expanded with the help of a balloon, the newer designs are self-expanding. The state of the stent struts is also an important factor. If they have bigger - $> 5mm^2$ - cell free areas, tissue may go through this 'holes'. If the stent structure is too rigid it may bend the vessel. [20] Another decision to be made before surgery is if a bare-metal stent (BMS) or a drug-eluting stent (DES) is used. There are many studies regarding the difference of BMS and DES. [21]

Stenting a branched vessel is not so easy because two stents need to be inserted, which is called kissing stent. They have a bigger discrepancy between the vessel wall and the stent mesh. A covered endovascular reconstruction of the aortic bifurcation (CERAB) reduces the radial mismatch. An unibody stent-graft shows even better results in following the bifurcation of the vessel. [22]

When stenting an aneurysm a new approach is to use stents with a woven mesh incorporated. This should prevent the flow entering the aneurysm area and therefore reduce the growth. [23] Another technique to prevent blood flow in an aneurysm is to use a coil, which is inserted into the protrusion of the vascular wall by different techniques. [24]

A big risk after stent implantation is the stent thrombosis (ST). Even though the incidence level is very low, if it occurs it can be fatal. Studies can also not make concrete assumptions after which time post surgery they will appear. [25] They can appear due to small injuries during implantation or due to platelet clumping on the struts or in dead space. The prevention and guidelines regarding ST are always changing and are inconsistent. So the treatment must be chosen individually for the case. But an important treatment is a dual anti-platelet therapy (DAPT). [20] New stent designs are also investigated to further prevent complications during stenting. [25]

2.3 Particle Image Velocimetry

In this section the most important background information for the Particle Image Velocimetry (PIV) will be discussed. Such as the general physical background, the micro PIV system and the 3D system. PIV systems and parameters for gases will not be discussed, as this is not important for the experiments in this thesis. If there is an interest in any additional information the book, Particle Image Velocimetry, from Markus Raffel, Christian E. Willert, et al. [26] is recommended.

The PIV is an optical non-intrusive velocity measurement technique. This means that the flow of the fluid will not get disturbed by inserted sensors, unlike direct measurement techniques, but rather tracer particles are mixed into the fluid. The PIV system then calculates the velocity from the measured displacement of the added particles [27].

In order to get the data for the velocity computation, two laser pulses are used to illuminate the particles in the test setup. The first one is set at the point of time t_0, the second one is then set after a time Δt, which leads to a second point of time $t_0 + \Delta t$. The particles then scatter the light of the laser and a camera is used to take a picture for each laser pulse. For better illustration, the schematic setup of a 2D PIV experiment in a wind tunnel can be seen

in 2.4 [27].

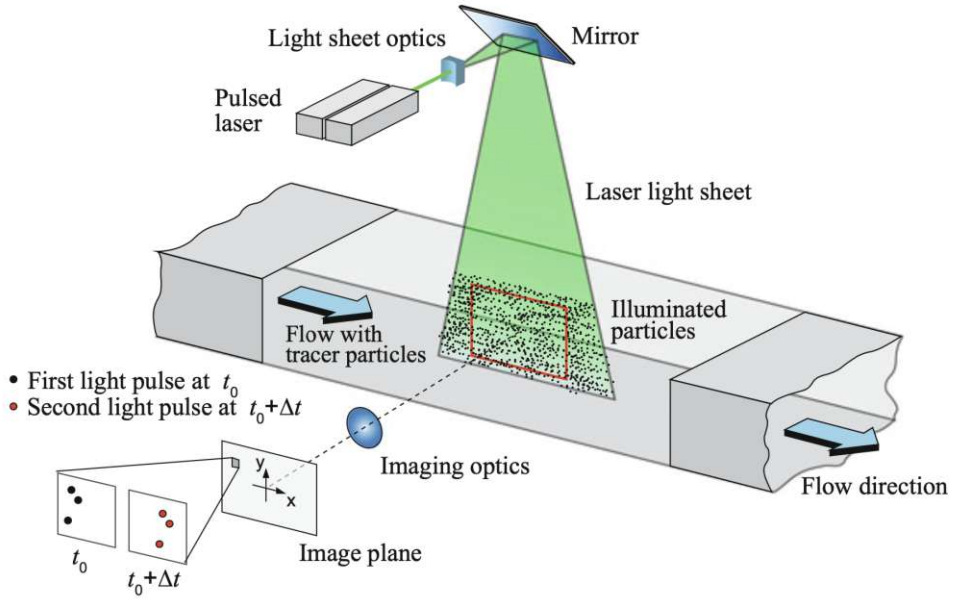

Figure 2.4: A schematic diagram of an experimental setup for a 2D PIV measurement. [27]

The PIV system is highly complex and there are a lot of parameters, such as tracer particle properties, illumination and the optical setup. Those can alter the quality of the images and as a consequence the results of the measurements. The parameters, which appeared to be the most important in this thesis, will be discussed in the next sections.

Tracer Particles

The tracer particles are a key component for the PIV system. Therefore, the selection must be made carefully. STOKES' drag law is a good way to find the best size for the used fluid. It considers the acceleration $\mathbf{a}$, the density of the particle ρ_p and its diameter d_p^2, the density of the fluid ρ and its dynamic viscosity [28].

$$\mathbf{U}_s = \mathbf{U}_p - \mathbf{U} = d_p^2 \frac{(\rho_p - \rho)}{18\mu}\mathbf{a} \tag{2.1}$$

With this parameter the velocity lag $\mathbf{U}_s$ can be calculated. It is the difference between the particle velocity $\mathbf{U}_p$ and the velocity of the surrounding fluid $\mathbf{U}$. This indicates how good the particles can follow the motion of the fluid. Tracer particles with very low sedimentation fit the best. If the density of the particle and the fluid is the same, it is called neutral buoyancy.

This means that no particles will set over time in the prob during testing [28].

Other important features of the tracer particles are the density and distribution inside the fluid. Density in this case means, the quantity of particles put inside the fluid which will later be tracked in the pictures. If there are to few it is not representative and when there are too many the software can no longer tell them apart. The particle distribution should be homogeneously in order to not change the local density in the recordings. This can lead to particle hot spots or no particle at all, as well as wave like particle density. Both would influence the results negatively. The best way to ensure a good distribution in the fluid is to stir the tracer particles in before the fluid enters the test channel [28].

When a very small particle size is chosen, the equipment should also fit the requirements. If the particles are too small, they can not be detected. There are particle which are recommended because of there light scattering behavior, but in the end the particles have to be chosen individually for every experimental set up.

Light Source

The most important properties of a light source used for PIV is the monochromaticity and the high energy density of the light. Therefore, lasers a widely used for experiments, but also light emitting diodes or white light sources can be used if they fit the setup. Lasers can be distinguished by their material, pumping source and mirror arrangement. The most commonly used lasers for PIV are argon-ion, semiconductor, neodym-YLF and neodym-YAG laser, the latter of which is used in this thesis, the nd-YAG laser yttrium - aluminium - garnet crystals. The good thermal and mechanical properties and the high amplification make this type of laser the most used one for PIV systems [28].

Finally it can be said, that the contrast of the picture and the scattered light power are direct proportional. The scattered light depends on the size and shape of the tracer particles as well as, the orientation and ratio of the refractive indices. Therefore, the particles are important and should be chosen carefully before increasing the laser power [28].

2.3.1 3D PIV

Due to the more complex set-up the 3D PIV has more advanced requirements for the laser light, camera and evaluation software. Additionally, there are different systems, depending on the experimental assembly and the desired results.
The most common are the holographic PIV (HPIV) and tomographic PIV. HPIV uses the interference patterns the particles generate with the light source, while several different cameras are used for tomographic PIV. In this study the tomographic method is used. During which one light pulse from the light source illuminates the whole region of interest (ROI) and cameras in different angles collect the position data form the tracer particles. [29]

In figure 2.5 a flow chart and a graphic illustrate the procedure of a tomographic PIV measurement. The optimum ratio between the depth and the width of the field of view (FOV) is 1:4. Nevertheless, much more pulse energy is needed to illuminate the FOV. In general more than three cameras in different angles are used. During the calibration process the position of the different cameras in space (X,Y,Z) and the relation to the projection on an two dimensional so called image plane (x_i, y_i) is calculated. Afterwards, the cameras are ready to record the sample simultaneously. The software can now reconstruct the path of the particles with an algorithm. [29]

Typical camera arrangements can be seen in figure 2.6. The cross display (on the left) has the advantage, that the two outer cameras have a smaller angle than the ones in the linear set up. The focal plane and the mid plane should be aligned. If this so called Scheimpflug condition is not full-filled there could be negative affects during the reconstruction. To ensure the observance of the Scheimpflug condition prisms or a lens-tilt adapter can be used. These need to be adjusted during the calibration process. [29]

The seeding density for 3D PIV can be higher than compared to the one in the micro PIV system. Additionally, the loss-of-pairs condition can be neglected for 3D measurements. The further use of cameras can handle a higher density for reconstruction accuracy. For a use of four cameras this means that the concentration of tracer particles can be as high as 0.05 particles per pixel, with a particle size of 10 to 100 μm. [29]

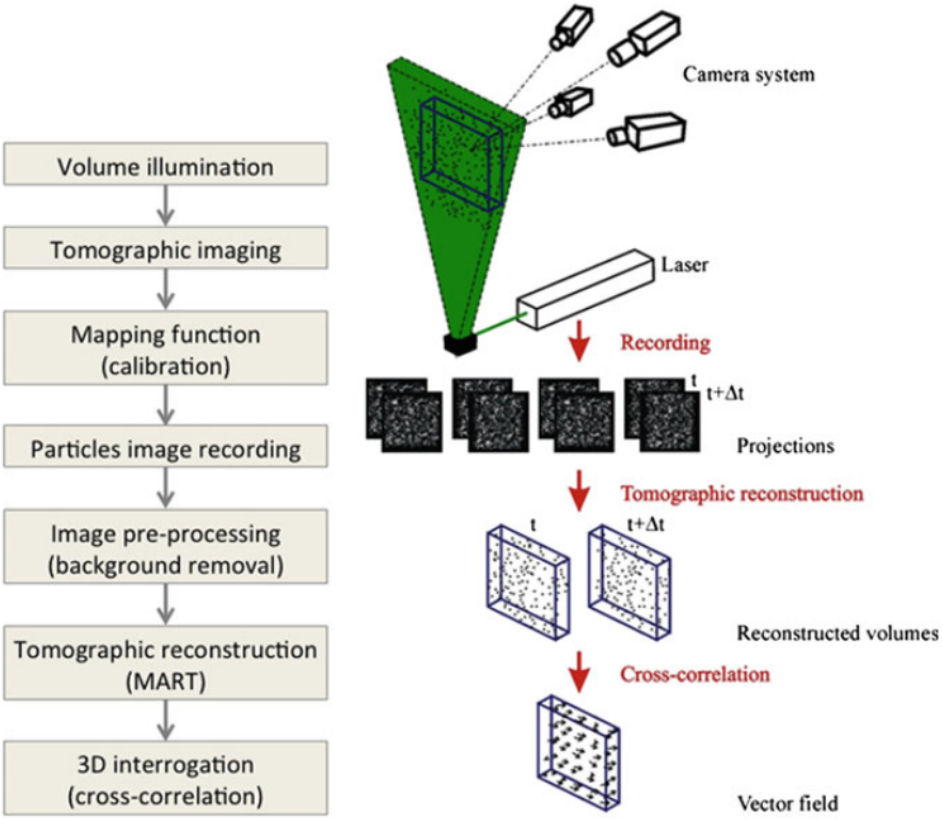

Figure 2.5: Flow chart (left) and a graphic (right) illustration of the procedure of an tomographic PIV measurement. [29]

2.3.2 Micro PIV

For micro-fluid systems the resolution of the standard PIV system is not high enough. Therefore a new system was invented by Stantiago et al. [30] in 1998. The micro-PIV system is a form of a planar PIV. The small size scale used in experiments with a micro-PIV can change the behaviour of the fluid. In continuum microfluidics, the fluid still behaves the same as in lager scales. While the behavior changes when the fluid is considered a sub-continuum. This can be explained due to the different scaling powers of inertia, shear stress or surface tension. Nevertheless, in typical μPIV systems only continuum microfluidics appear. The sub-continuum flows would be too small for visible light. [31]

The typical μPIV set-up has the same components as the regular PIV with the only exception of the microscope, as seen in figure 2.7. The camera and laser are attached to the microscope. Therefore, the laser pulse and the measured scattered light both take place through the same glass window. This is called a back-scatter configuration. To prevent to much interaction between the laser pulse and the camera a dichroic mirror or epi-fluorescence prism cube is used

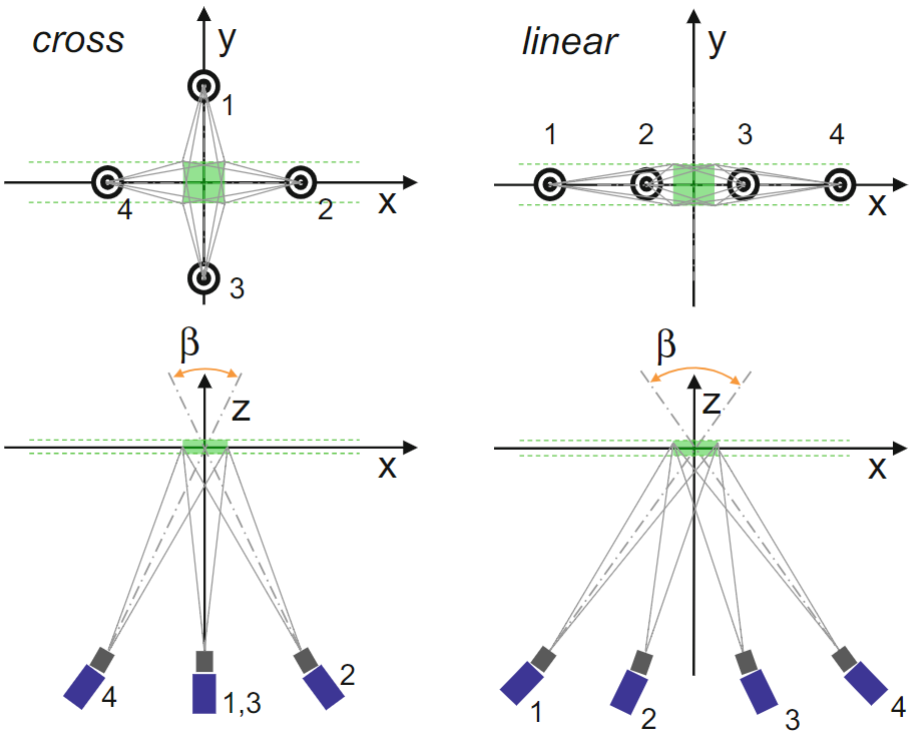

Figure 2.6: The two typical camera arrangements for the 3D PIV. On the left hand-side a cross system and on the right hand-side a linear set up. [29]

to separate the different wavelengths. Due to the smaller channel size a syringe pump is used to pump the tracer particles, which are as small as 1 μm, through the probe. Otherwise the flow could be driven by e.g. surface tension or gravity. The objective lens can be individually chosen for the experiment, depending on the ROI and the FOV. It must be noted, that the magnification must be high enough to display the tracer particles. The selected particles are of an acceptable size, if they do not show interaction with one another or the probe. This could lead to the clocking of the geometry. Additionally, due to the back-scatter configuration, particles with a fluorescing behaviour are used. [31]

2.3.3 Refractive index matching

The refractive index (RI) matching is important when light travels through different media. The light beam gets bent varyingly strong. The light enters through medium A and gets bent at the boundary layer to medium B, as illustrated in figure 2.8. If the refractive index n_A and

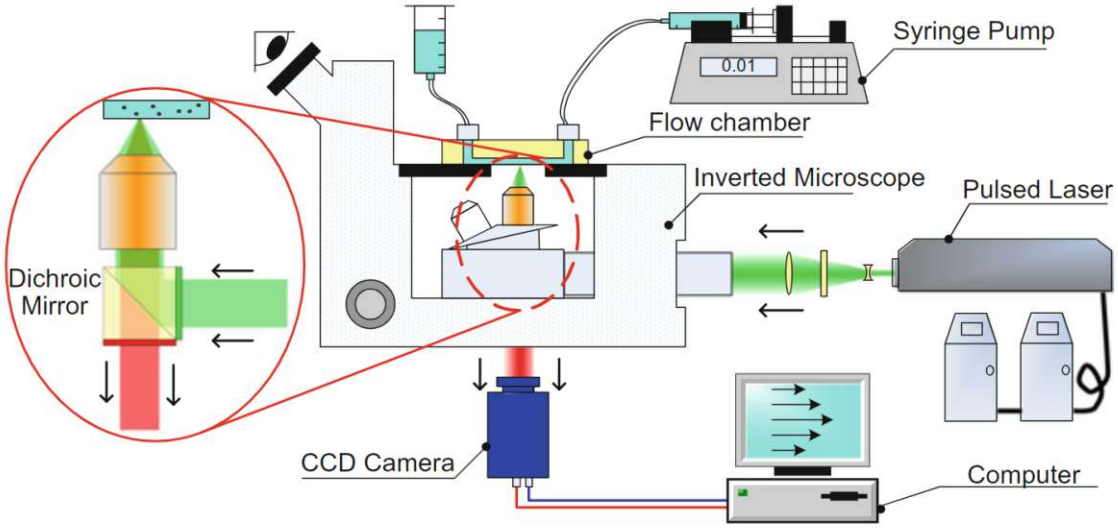

Figure 2.7: A schematic depiction of an micro-PIV system. With a flow chamber, the laser beam and the combination of the microscope with the camera. [31]

n_B are the same, Θ_A and Θ_B would also be the same.

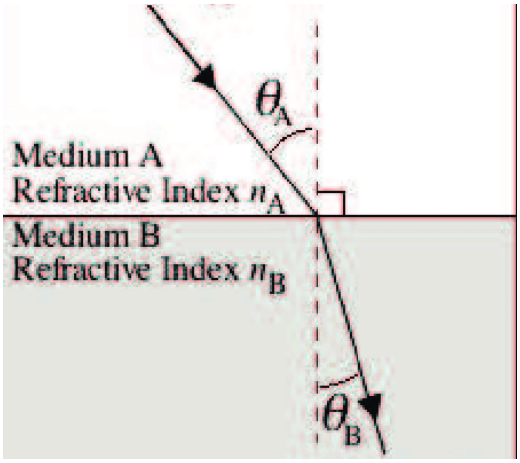

Figure 2.8: The light beam gets bent at different angles by the two media. [32]

For this experiment the light in the 3D PIV setup will travel through solid-liquid. For the curved surface of the cylinder the aquarium around the probe is very important. The same fluid must be put inside and around the model. After choosing the solid materials for an experiment the liquids needs to be picked. When mixing different liquids care must be taken for potential reactions. When the refractive index is measured it need to be done at the temperature the experiment will take place, because the RI can change with temperature. [33]

Table 2.1: The most important Refractive index values needed for this thesis.

material	Refractive Index	state	reference
Water	1.333	liquid	[34]
Glycerine	1.473	liquid	[34]
WACKER SilGel 612 A/B	1.404	solid	[35]
Formlabs Resin Clear	1.5304	solid	[36]

3 Materials and Method

In the following sections the methods to obtain the data for this thesis are listed and described. Starting with the design and prototyping of the blood vessel models, with different materials. After this the experimental setup, data collection and post-processing will be explained.

3.1 Part Design With CATIA And Formlabs

All designs were made with the Computer Aided Design (CAD) software CATIA V5-6R2020 (Dessault Systèmes, France). The designed parts were then printed with the formlabs SLA-printer form 2 (Formlabs GmbH, Germany). In the next section the process of designing and printing is explained. As a reference for the design the channel design from Kleedorfer L. [37] were used.

3.1.1 Channel Design For The micro-PIV

For the first drafts channels from a previous project were used as a size reference. Since the channels are open at one side, the size is also the same as the size of the microscope slides used to cover this side. At first the connections were on the long side of the block, see 3.1. This showed no good use during tests. The connectors leaked, even though paraffin strips were added to seal them. So the connectors were switched to the top of the part. Additionally, a Luer connector was added, this helps to connect the tube to the channel.

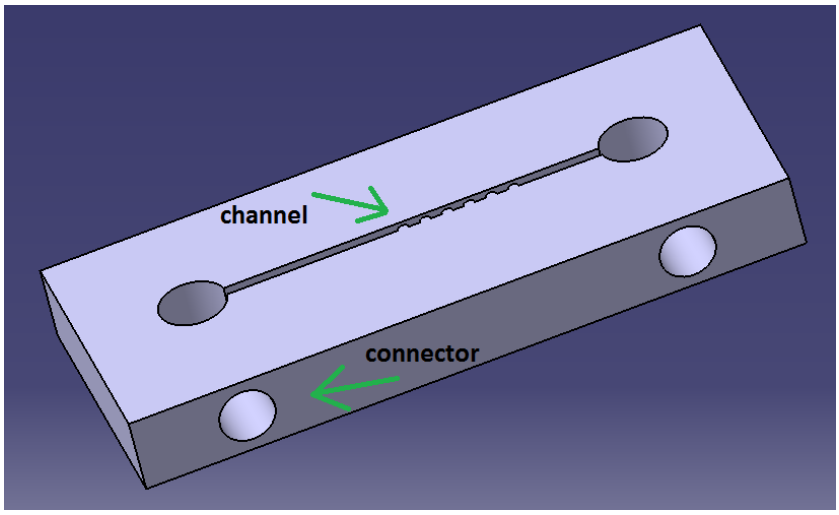

Figure 3.1: The first drawing of a channel for the μPIV system. The channel in the middle is open and the connectors are on the side.

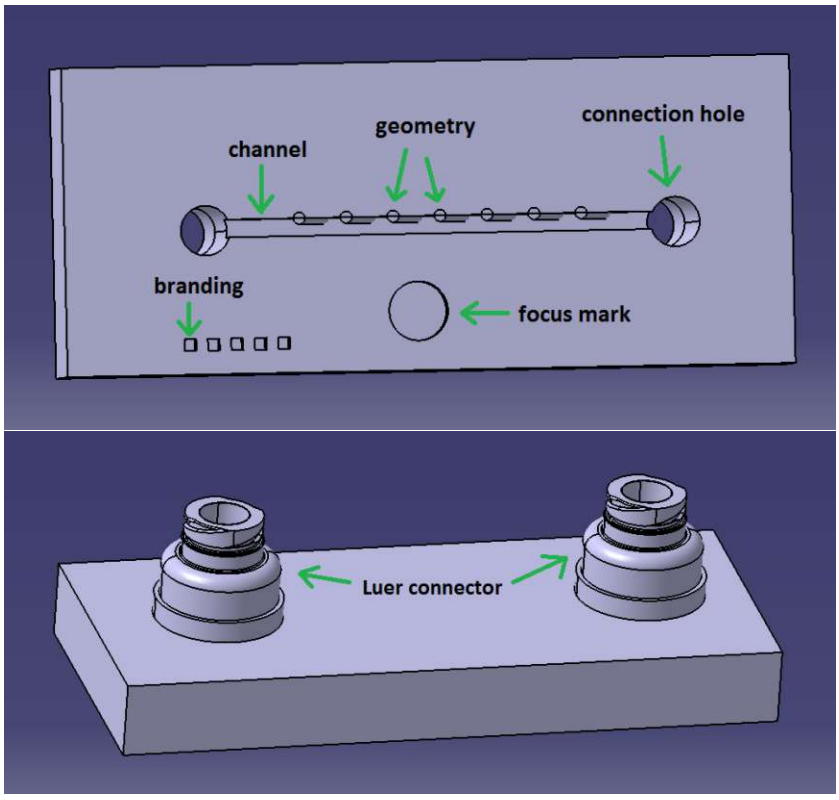

Figure 3.2: The upper picture shows the bottom, onto which the slide glass is glued on. The channel with the geometry, the focus mark and branding and the connection hole to the other side are tagged with green arrows. In the lower picture the front side with the Luer connectors is shown.

In figure 3.2 the final design can be seen. In the top picture the bottom is shown, with the channel containing the geometry, a branding for easy distinction between the different geometries, a focus mark for the experiments and the connection holes to the front. This side is open and will later be covered with a microscope slide, as said before. In the bottom picture

the top side with the Luer connectors is shown. The fluid will be pumped from one connector, through the connection hole, the channel, the other connection hole and out again through the second Luer connector. Before more geometries were designed, the channel was tested in the μPIV.

In the next step, different geometries are designed and added to the channel. For all geometries semicircles are used to simulate the stent embedded in the blood vessel wall. To investigate different stages of in-growth of the stent into the vessel wall, three different versions, from half-circle to full circle were printed. Pictures of the different circle positions can be seen in figure 3.3, the different stages of flow obstruction is highlighted in green. After different problems during the printing, the channel size was finally enlarged to 3 mm. The circle radius is 0.5 mm, with a 3 mm distance between the centers of each circle.

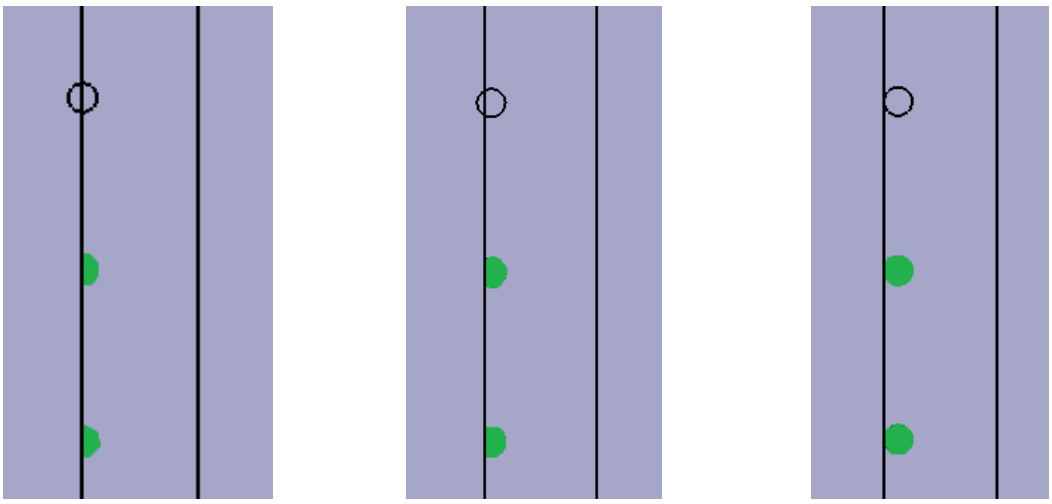

(a) (b) (c)

Figure 3.3: Three different stages of stent in-growth. (a) shows only a half circle, implementing that the stent is completely embedded in the vessel wall. (c) shows a "fresh" inserted stent while (b) shows a stage between the other two.

Not only different stages of in-growth are of high interest in this thesis. For a better simulation of the stent design, not only straight but also angular or even X like shapes were drawn into the channel. Three of these designs can be seen in 3.4. The channel is cut in half to make the geometries, highlighted in green, visible. From left to right they show a straight line, an angular line, simulating a helix, and an X form, simulation a double helix. The designs were done with a 0.5 mm radius. The angles used for the X formation were 45 °, in both directions. While

30 ° and 50 ° were used for the tilted single cylinders.

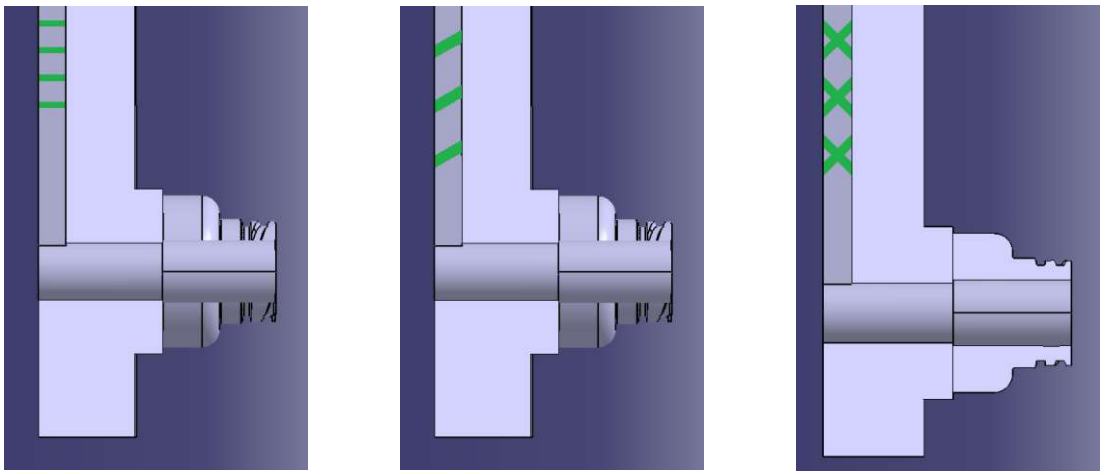

(a) (b) (c)

Figure 3.4: The green highlighted structures in the channels show different stent like designs. The complexities get higher from left (a) to right (c).

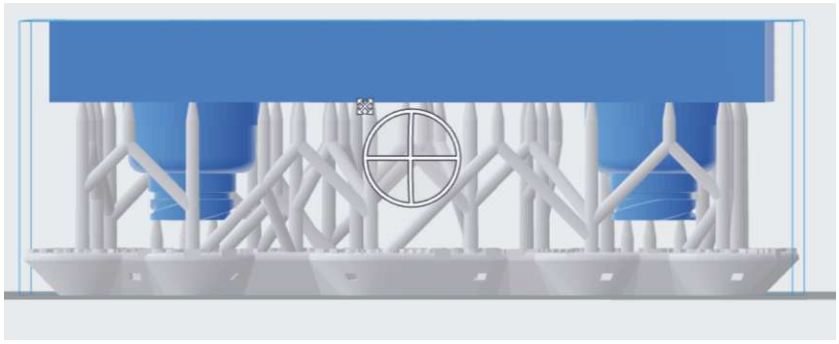

Figure 3.5: Close up of a channel in the printing interface. The blue part is the channel and the light grey mesh shows the needed support structure. The white circle in the middle is a tool to move the component.

Printing Process

All the channels were printed with the smallest possible coat thickness of 0.025 mm and the Clear V4 resin. With the PreForm software the .stl files of the designed channels could be placed for the printer. As seen in figure 3.5 the orientation of the part in blue is shown. As it can be seen, the Luer connectors are facing down, but during the printing process this will be the other way around and the connectors are printed first. This ensures, that there is no resin built up in the channels. Which could clog them, making them unusable. The grey support structures around the blue part is essential for a good print. This structure can be added automatically but in this case, all the points of contact as well as the size of this points is chosen individually.

Around the Luer connector fewer points with a size of 0.4 mm were preferred, in order to minimise the chance of damage during the post processing. In figure 3.6 the difference between

a Luer connector which was attached to support structures on the left side and one without connections on the right. The upper edge on the left one is clearly damaged. While the edge on the other one is level and without any damage. Unfortunately, for the channel used in the μPIV it is necessary to put support structures on the Luer connector. With a radius of 0.3 mm for the connection points the printer was not able to print the Luer connectors, but the rest of the structure. What this would look like can be seen in the following figures. In figure 3.7 the supporting structure is still attached to the channel but the Luer connector is clearly missing, marked with a red circle. This makes this channel unusable. In figure 3.8 the support structure is removed. The missing Luer connector was floating in the tank of the printer. This implements, that the weight off the Luer connector got to heavy and it fell of before the printer could add the rest of the block.

(a) (b)

Figure 3.6: A slightly damaged Luer connector (a) and a Luer connector with no damage from post processing (b).

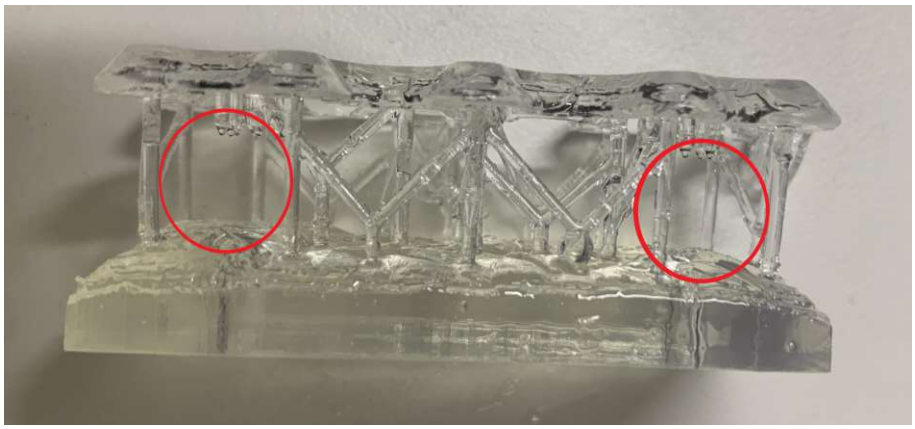

Figure 3.7: A failed print with the support structure still attached to the channel. The red circle marks the place of the missing Luer connector.

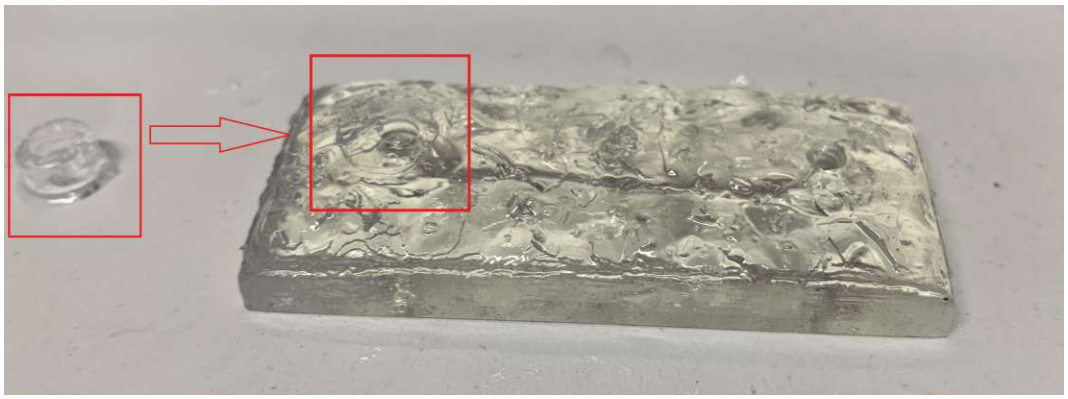

Figure 3.8: An unusable channel after the supporting structures are removed. The red rectangular marks the Luer connector, which should be on the top of the channel.

On the rest of the channel points with a bigger radius, mostly 0.8 mm, are used to make sure, that the structure is well supported and does not fall from the building platform. The software also checks, if the support structure is good enough for the print and will color the part red when more points of contact are needed. After the software showed, that everything is good for the print, the parts were copied as often as needed. In picture 3.9 the PreForm interface with four structures ready for printing is shown. The chequered area symbolizes the building platform of the printer. Again, the print will be reversed to the images the interface shows.

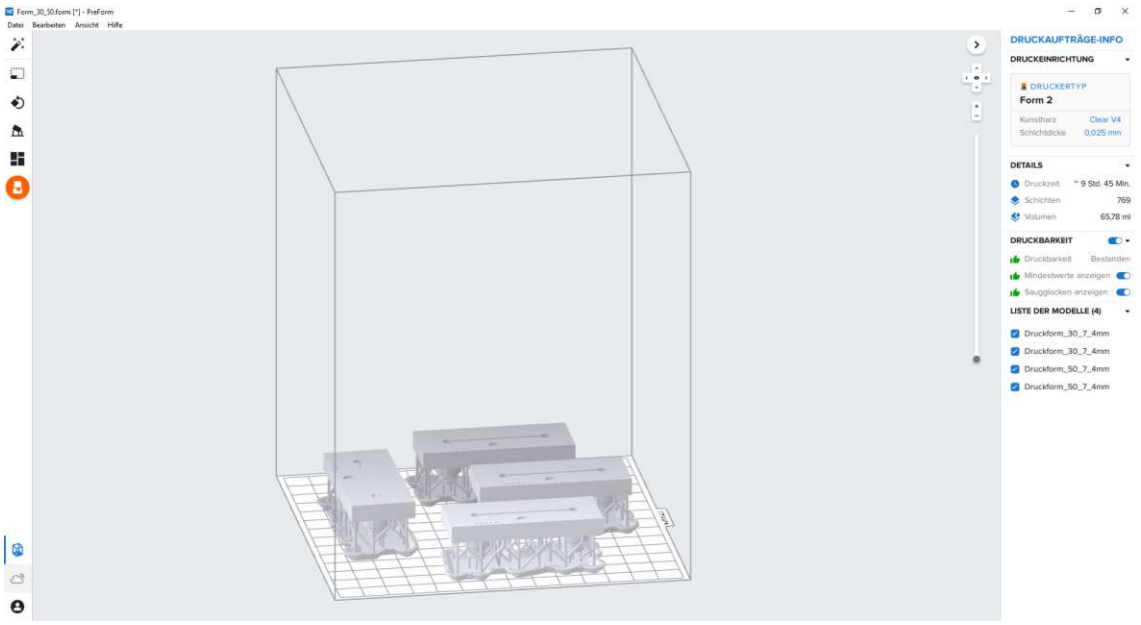

Figure 3.9: The interface of PreForm with four channels ready for printing. On the right hand-side the most important info is shown. In this case the Clear V4 resin is used with a coat thickness of 0.025mm.

As said before, the printer clogged channels if they were too thin. Additional, for some prints the width of the channels was too small for the chosen radius of the circles. This also resulted in clogged channels. This can clearly be seen in 3.10. These samples are unusable. The fluid has no chance to flow. As the circles have a radius of 0.5 mm the width of the channel was also enlarged, to ensure a good flow.

The printer also seemed to have some troubles printing in good quality if the circles were too close to each other. In figure 3.11 this problem can be seen. The distance between the circle centers in the upper channel is 2 mm, making the distance between the edges of the circle 1 mm. This was too small for the printer and the resin built up between the circles. To avoid this the distance was enlarged by 1 mm, as seen in the lower channel. The circles all have sharp edges and the space between them is not filled with resin.

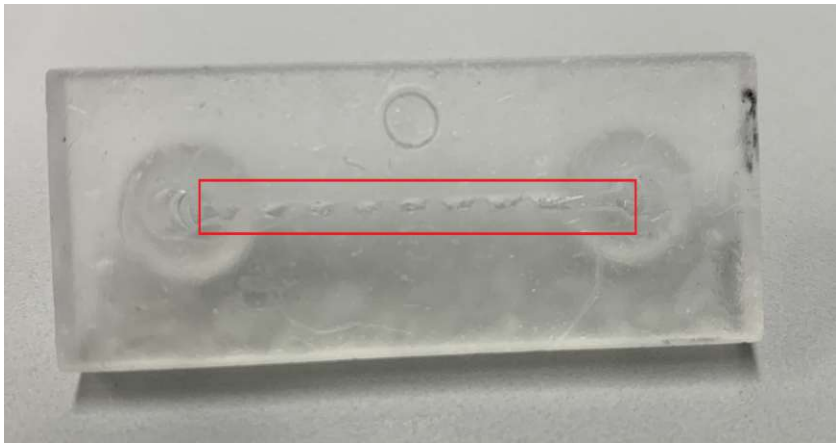

Figure 3.10: The width of the channel was too small and it got clogged with resin during the printing process.

3.1.2 Design For The 3D PIV

The design process for the samples used for the measurements with the 3D PIV started with a simple hollow cylinder. These cylinders were printed with different wall thickness, a various amount of support structures and in different orientation. In order to test the limitations of the printer. The wall thickness varied from 0.25 mm to 1 mm. Thicker cylinders are more stable and rigid, but less transparent. The thinnest walls had holes and other mistakes. An example can be seen in 3.12, the wall is too thin and the cylinder collapsed, even though a support structure was used. It could also be observed, that structures which were printed standing up showed a

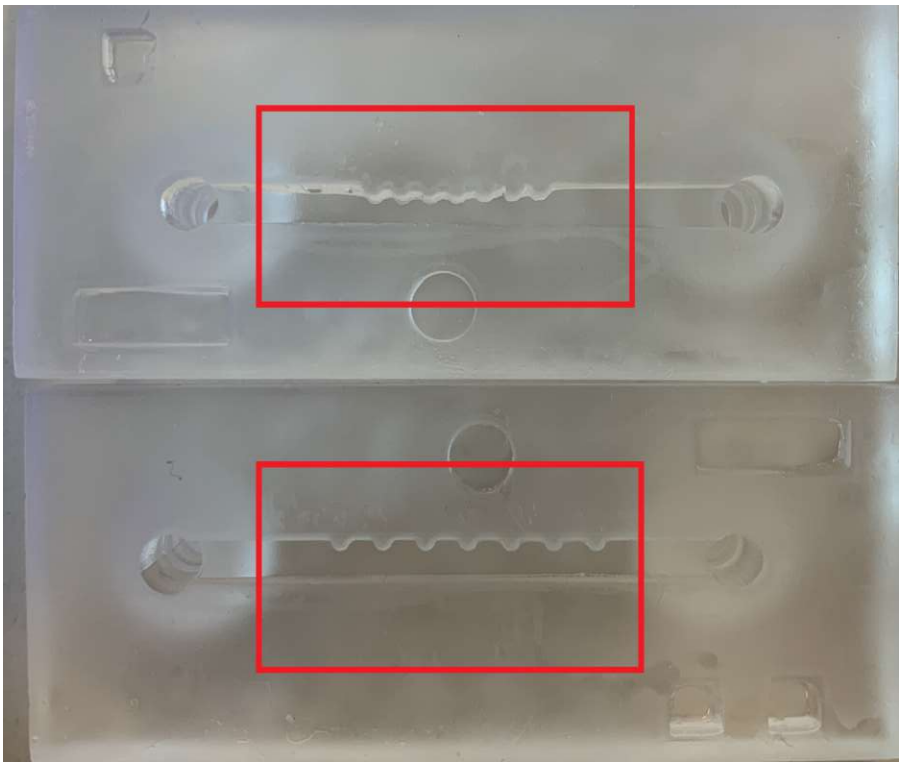

Figure 3.11: The upper channel has a distance between the circle centers of 2 mm, the lower one has a distance of 3 mm. As it can be seen the printer was not able to print the circles too close to each other.

better overall image, than the ones laying down. The use of different support structures was also tested. Unfortunately, the structures did not only deform the cylinder, when they were placed inside the hollow form, but also could not be removed. Figure 3.13 shows the difference between a cylinder with inner support structures, on the left, and without, on the right. After this observation it was decided to place the support system only on the outside of the design.

Afterwards, one challenge was the fixation of the cylinder into the 3D PIV setup. The whole setup will be discussed later in the section 3.3. As the same tube system was used, as in the μPIV experiments the Luer connector had to be incorporated. The section with the helix is only 2 cm long and therefore plane cylinders were added before and after to make the sample larger and give the flow time to develop. The sudden pipe expansion from a diameter of 5 mm, at the Luer connector, to 10 mm, at the cylinders, would bring turbulence into the flow. Therefore, a diffusor for a graduate change in pipe diameter is needed. To underline the importance of this, G. Satish et al. [38] did a simulation to show the difference in flow and pressure changes for gradual and sudden changes in pipe diameter. The pipe diameter was 1:2 for the smaller and larger diameter. It can be observed, that the pressure increases, while the velocity decreases.

Figure 3.12: The cylinder collapsed after printing, due to too think wall thickness.

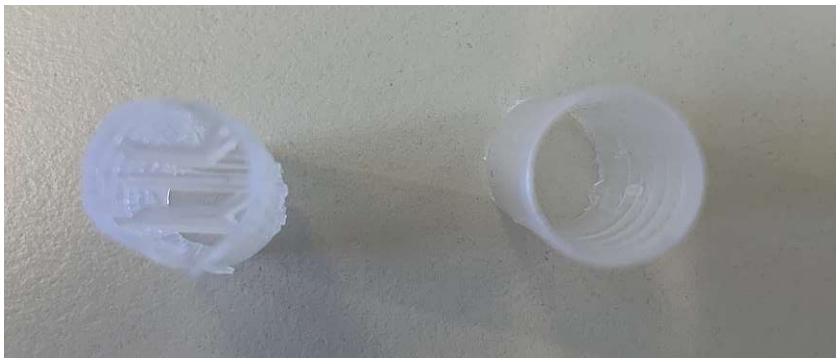

Figure 3.13: Two different cylinders with different support system. The left cylinder was printed with inner support structures, while there were only used support structures on the outside for the right cylinder.

This must be considered when choosing the flow-rate of the syringe pump in this experiment. In figure 3.14 the relationship between the diameter, the length and the diffusion angle can be seen. With the trigonometrical connection of the tangent of the triangle the length and $\Delta R = R2 - R1$ - in reference to figure 3.14 - the diffusion angle was calculated. The size of the angle is important, as a smaller angle avoids separation and reverse flow. In different studies it has been proven, that a smaller angle results in less back-flow. The optimal angle is between 7 - 8 °. [39][40] With a small diameter is 5 mm, a bigger 10 mm, the length has to be 20 mm to receive an diffusion angle of 7.688 °.

The diffusor was implemented with CATIA. By doing this, all different parts needed for the test tube are finished. In the next step they are assembled according to figure 3.15. Even though

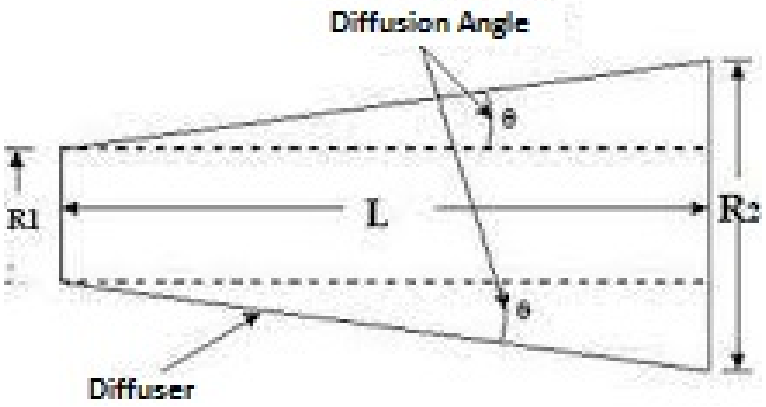

Figure 3.14: A schematic picture of a diffuser [41]. For this experiment R1 = 5 mm, R2 = 10 mm, L = 20 mm and the calculated diffusion angle $\theta = 7.688$ °.

the printer was able to print the tube with a wall thickness of the geometry part of 0.5 mm, it had to be thickened to 0.6 mm. After this alteration and the reduction of the helix whorls from 10 to 5, the printer hat no more problems in printing the tube.

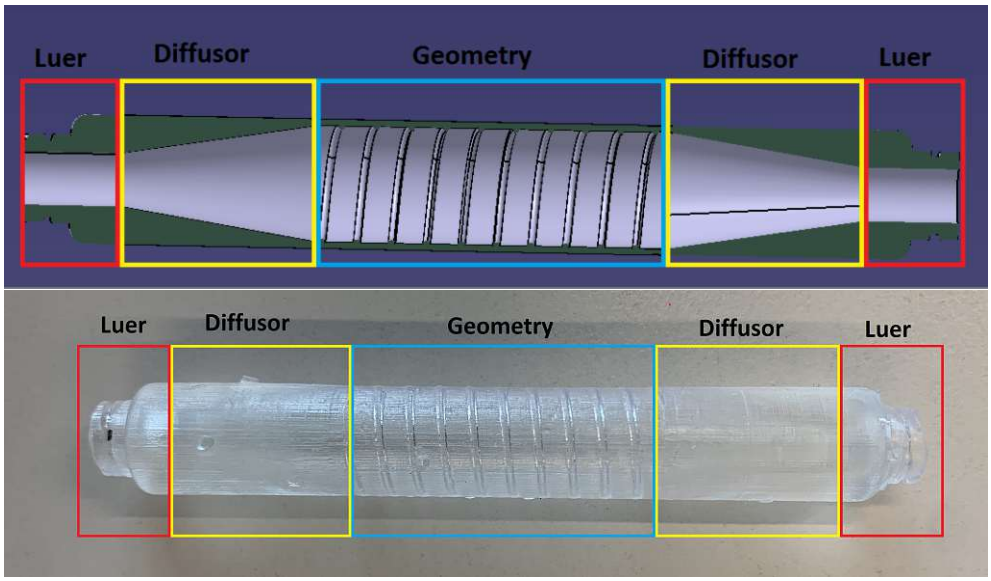

Figure 3.15: The upper figure shows the cross section of the cylinder, in the CATIA interface. The lower picture is the some cylinder after the printing. In both pictures the structure is highlighted for better comparison. On both ends are Luer connectors, then the diffusor and in the middle the geometry.

To ensure that the resin could exit the tube during the printing, these were printed standing up straight. Figure 3.16 shows the structure, blue, with support structure, light grey, in the printer interface.

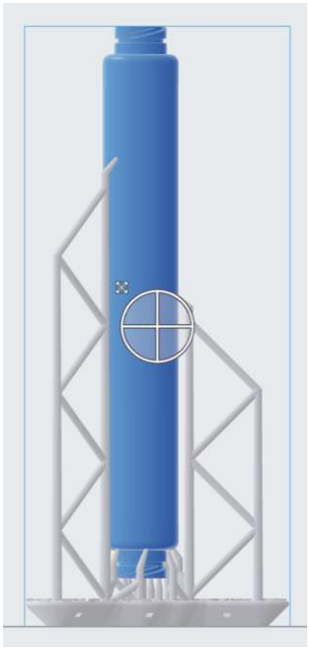

Figure 3.16: Close up of the cylinder in the printer interface. The structure, blue, is surrounded by support structure, light grey.

As mentioned before, the printer had some difficulties with the design, even though all three of the prints in figure 3.17 were printed at once and exactly the same, print **A** is missing the hole geometry, print **B** has a slit and print **C** is looking good, but it also has small wholes inside the wall and is therefore useless for the experiment. But with the changed design this problem was gone.

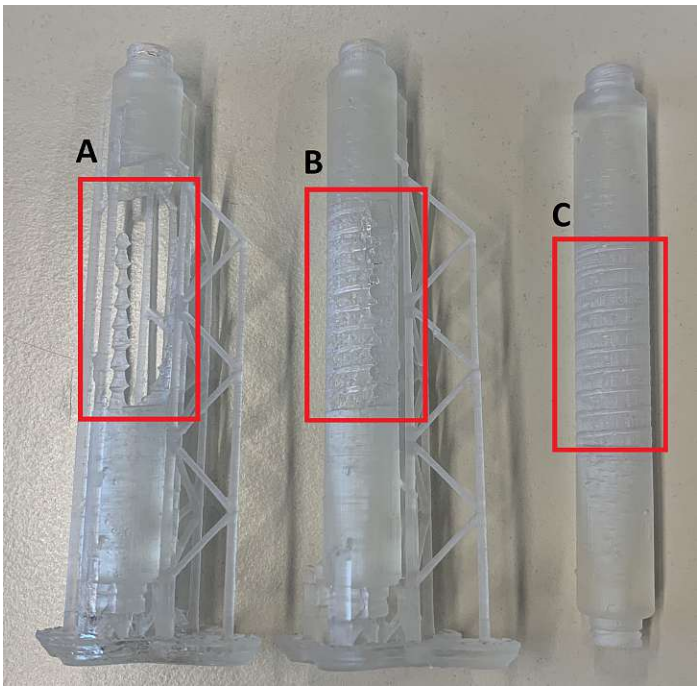

Figure 3.17: Printed structures with mistakes. A - the whole geometry is missing. B - a slit is visible on one side. C - looks good, but has small holes inside the wall.

Another approach was to just print the Luer connector combined with the diffusor. This part can than be used to put cylinders from different materials into the experimental setup. Therefore, the diffusor had to be slightly adapted. A small overhang was added to the diffusor, in order to glue the cylinder flush into the part and avoid small holes on boundary layers. In this case, the diffusor has to be adapted for the different cylinders, as they could had different outer and inner diameter and the connection should be as smooth as possible. Additionally, a cuboid was added around the test geometry. This approach was made by Stanley et al. 2023 [42].
This design was also used to test if the formlabs print with the clear resin shows better results if the parts get coated with a varnish. The clear coat (Life Colours Klarlack glänzend, Elita Modelle e.K., Großhabersdorf, Deutschland) is sprayed on with an air brush gun after post processing the the cylinders. After two cotes a small layer of superglue is added on the rim and an adapted connection tube is pressed onto both ends. The difference between the cylinders before and after coating can be seen in 3.18. **A** shows the untreated cylinder and **B** shows the finished part.

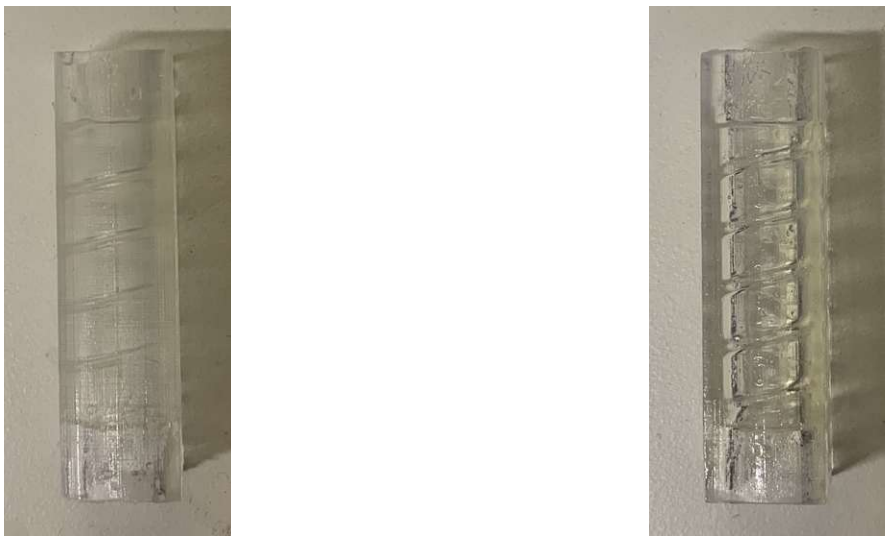

Figure 3.18: Image **A** shows the cylinder after post processing but without another treatment. Image **B** shows the cylinder with 2 layers of clear coat.

3.2 Silicon Mold

To better mimic a blood vessel and to ensure the laser will not be blocked by the material, silicon was selected as the material of choice for a 3D model for the PIV system.

For the first test a simple form was milled into a Teflon and a metal. The silicon used is the two components SilGel® 612 A/B (Walker, Germany). The solution was then mixed in the ratio A:B equal to 1:1 as recommended. The forms were placed in an 100 °hot oven, to enhance the setting. However, troubles were faced with the consistence of the hardened material. It was too sticky, which led to difficulties during the demolding process. Hence, it lost its shape once removed from the form. The information on the Walker homepage stated, that an increase in component A leads to a harder and less gummy result. On that account, the ratio was changed to A:B equal to 1.5:1. This ratio showed way better results, in the same mold, and the silicon was easier to remove. The shape was still intact and the surface was not too sticky. Even small details, like the grooves from the milling, are perfectly shown.

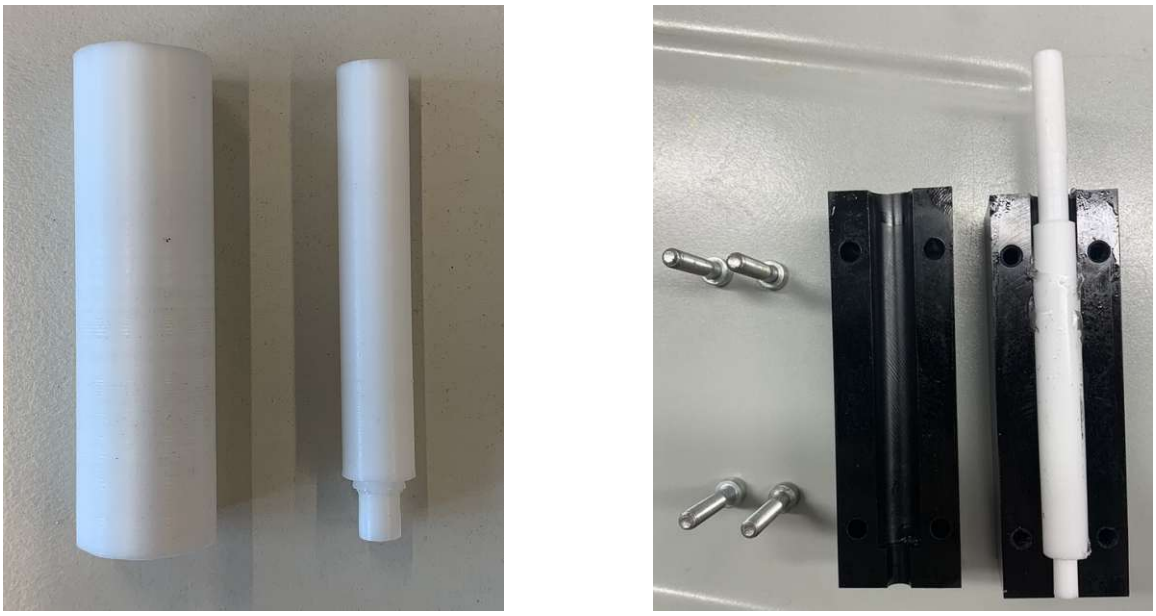

(a) (b)

Figure 3.19: The two pictures show the difference between the first figure (a), with an cylinder which cannot be opened and the second figure (b) design of the mold, in its opened form.

In the next step a cylindrical Teflon form was manufactured. It consists of an outer and an inner removable cylinder, as seen in picture 3.19a. The first molding test with this design was not very successful. The silicon lost all its form, as the friction due to the stickiness was too

much. After the second try, the silicon was again placed in the oven. The results were alike as with the previous pour. The demolding was difficult and the silicon was sticky and only half of the tube was intact.

In the next step, the form was redesigned, see 3.19b. The outer shell consists of two polymer parts which are fixed together with screws. The inner cylinder was adjusted and again made of Teflon. This new design element should help with the demolding, additionally a release spray was used. For the next tests a new silicon was ordered, as the other one reached its expiration date. The new silicon was mixed in a 1:1 and a 1.5:1 ratio, but the mixture with the higher amount of part A showed better results. If the ratio of part A was even higher with a 2:1 ratio the problem with the stickiness came back. Then the silicon does not get hard and sticks to the outer shell. What this means exactly can be seen in 3.20c. Additionally, the form was placed into a ultrasound water bath after it was filled. This helps to minimize the number of air bubbles in the silicon. If the form was not put into the ultrasound bath large in-closed air bubbles appeared during the demolding, picture 3.20a. When the form was filled to the top an overflow, picture 3.20b, after placing the full mold into the oven occurred.

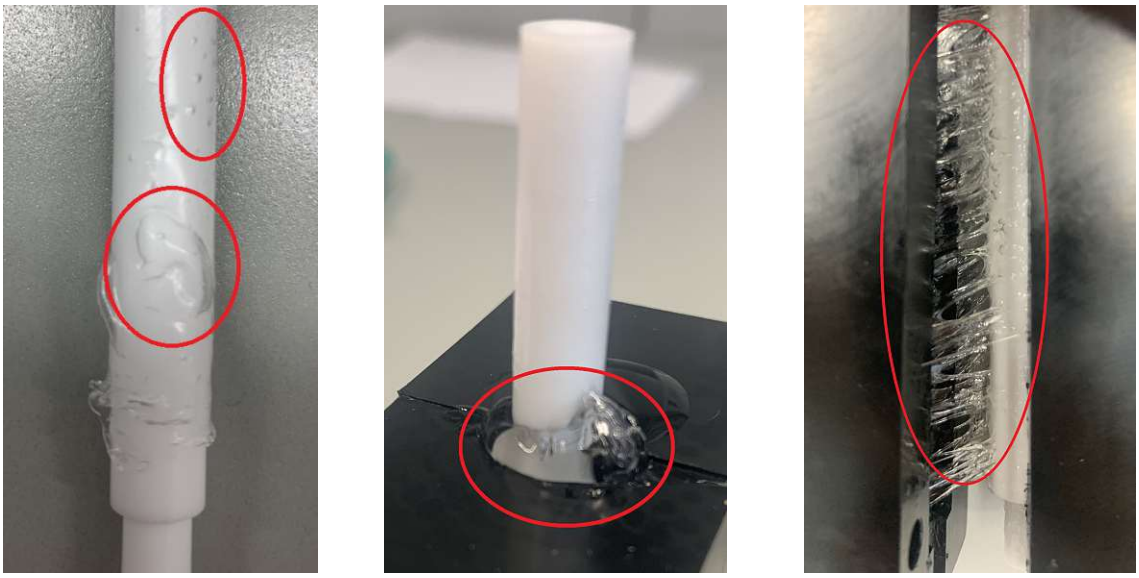

(a) (b) (c)

Figure 3.20: In picture (a) lager air bubbles and wrinkles can be observed, marked by arrows, picture (b) shows an overflow, red circle, and in picture (c) the curing process was not optimal and the silicon is stuck on the outer shell of the mold.

Unfortunately, no usable sample could be produced with the new design. The silicon shell was too thin and ripped easily. Figure 3.21 shows the only sample which looked like a tube, but it also ripped at some places. After some more research the lost-wax technique was used, as a reference the studies from [43] and [44] were used as an inspiration. A simple drawing of the new idea can be seen in figure 3.22.

Figure 3.21: A demolded silicon tube. The ends are fringy and the tube is not complete.

For the new design a fist prototype was made of an existing metal profile and a metal plate, where the profile was fixed on with 3D printed holders, see figure 3.23 In this form a wire with a wax cylinder was added through two holes on the short side of the form. Molding wax was pressed onto a wire and than placed inside the rectangular metal profile. Additionally, small connector tubes, printed with the Form 2, were added into the wax. This had the goal to investigate how good the printed material inheres on the silicon. These connectors consisted of the same Luer-connector and diffuser as the printed tubes for the 3D PIV samples. This structure than would be used as a connector for the tubes and syringes in the same way as

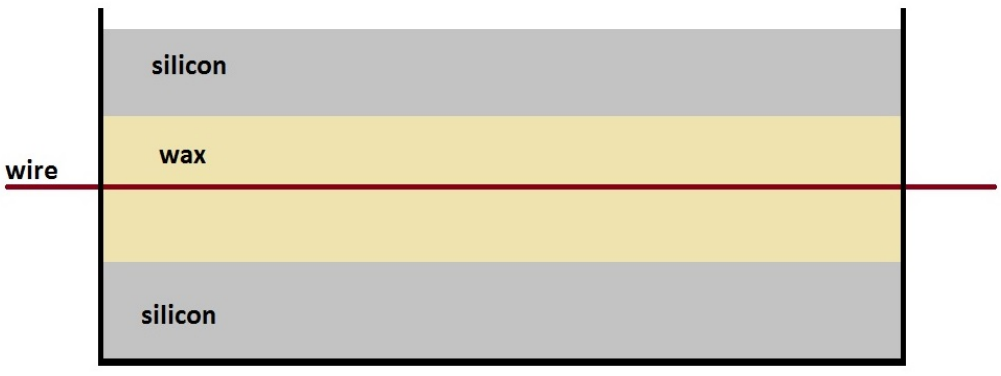

Figure 3.22: A simple drawing of the new mold for better understanding. The wire can be removed and is used to hold the wax in place when the silicon is poured around it.

it is in the printed tubes. As the fixation of the silicon sample into the 3D PIV set up was a big question with the previous molds. The silicon showed better curing results than the tests before. However, the silicon around the printed structure would not harden. This can be caused by remains of Isopropanol or not fully cured resin.

The form could be demolded by removing the 3D printed holder and the profile from the plate before pushing onto the silicon from from one side. This was quite difficult and left a lot of fingerprints on the silicon. To remove the wax a hairdryer was used. The wax got soft and could be pushed out of the form. Afterwards the remaining wax was blown out as much as possible. Additionally, bowling hot water was purred into the holes of the form to remove even more wax.

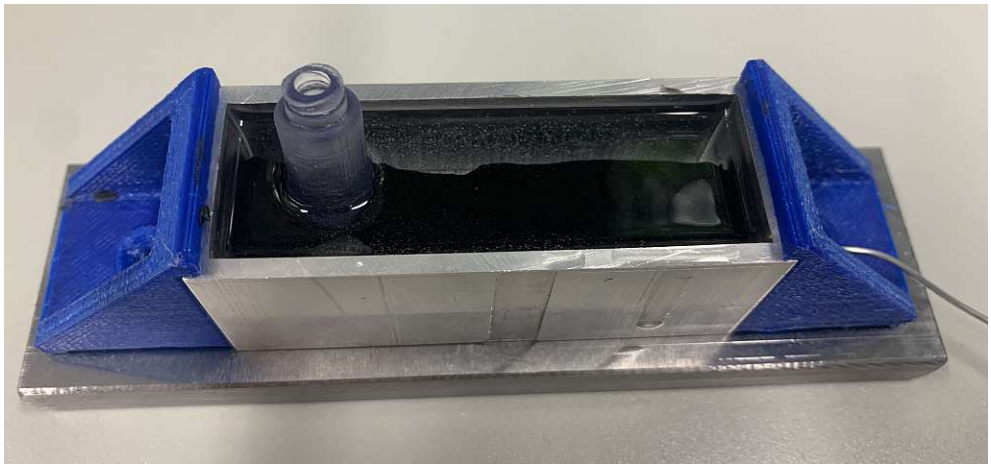

Figure 3.23: The prototype of the new design. The black cylinder in the silicon is the wax, with a printed connector tube pushed into it. The blue forms hold the metal profile in place on the plate.

Before a new design was manufactured the printed connectors were treated in three different ways. If the silicon would not harden around the printed parts after the treatment a new way would be needed. The first treatment was putting the part into a UV chamber - **A**. There it would fully cure for 120 min at 80 °. A second part was simply washed with water and dish detergent - **B**, to make sure, that no residue from other substances was left. For a third connector a clear coat spray (Marabu Klarlack, Marabu, Tamm, Germany) was used - **C**. After spraying the part form all directions it was placed to fully dry. The three parts were then stuck to the bottom of the form with wax. The silicon only cured completely around part **A**. Around part **B** and part **C** schlieren are still visible. Top image in figure 3.26. On the bottom image of the same figure, red circles mark the gap between silicon and part, after they were tilted, only

part **A** shows no space. This led to the result, that all printed parts used for the silicon mold have to be put into the UV camber before they could be used.

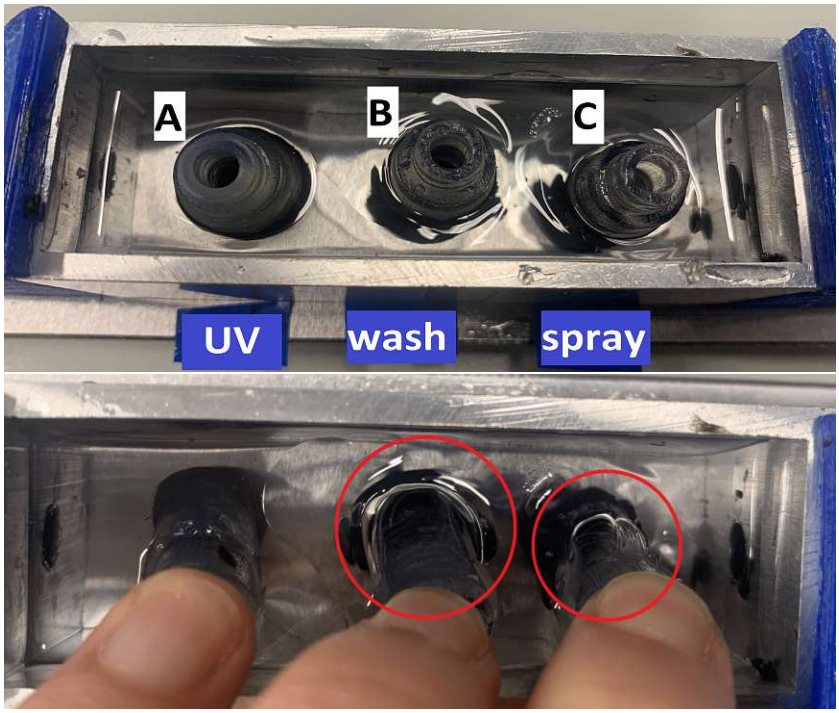

Figure 3.24: Printed connector in silicon after using different methods of post processing. **upper image:** A - part was placed in the UV chamber. B - part was washed. C - part was sprayed with clear lack. **bottom image:** The red circles mark a gap between silicon and tube.

To give the silicon even better chances to really stick to the printed part, a 10 mm high helix was added, see image 3.25. The slightly tilted geometry of the helix should have a similar effect as barbs, to make sure the silicon will not slide off of the connection tubes.

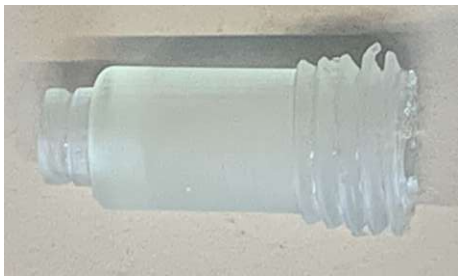

Figure 3.25: The final design of the connection tube for the silicon casting.

The final design of the silicon mold is composed of five individual metal plates. Holes with the same radius as the connectors were drilled into the short side of the metal plates. Hence, they could be placed in the form for good cooperation into the silicon casting. The plates are then put together by screws. In the top image of figure 3.26 the part can be seen. The connection

tubes are placed in the same way as they would be during the pouring process. In the lower image of the same figure only two laterals are fixed together.

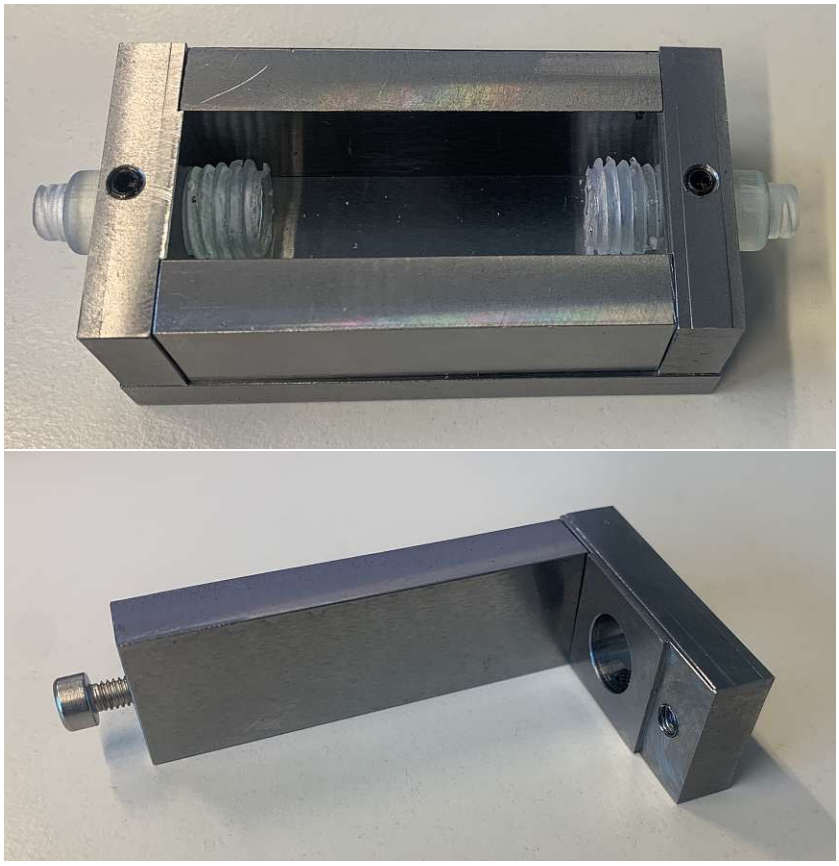

Figure 3.26: The final design of the silicon mold. The upper picture shows all parts of the mold put together. Additionally the connection tubes are put inside their holes. The lower one displace only two side walls fixed together.

All the lateral walls were unscrewed, except for one longer side. Then a cylinder was made from wax, a little wooden stick was placed inside to give the wax a strut. It was rolled until it had the same diameter as the connection tubes. The wax cylinder was cut to the same size, as the space between the connection tubes inside the cast. The connection tubes and the wax mold were pressed together before they are placed into the holes of the shorter sides, which were mounted back on the lower plate. In figure 3.27 this step can be seen. The orange cylinder is the wax. Now the last wall was fixed in place and small slits, between connector and form wall, were plugged with remainder of the wax. The silicon was mixed the same way as before and poured into the case.

After curing over night the base plate was removed. Afterwards the form was placed in a holder, to collect the wax, and the construction was placed inside a UV camber. The camber would reach a temperate of 80°and run for 2 hours. This constant high temperature should help to

Figure 3.27: The silicon form with the shaped wax cylinder, in orange, merged together.

remove the wax from the inside. In figure 3.28 the mold is shown after the UV chamber. Once the form was cool again, the screws were unscrewed and the plates were disassembled. The silicon stuck to the metal walls and it was hard to remove the plates.

Figure 3.28: The silicon form after the form was filled with silicon and put into an UV chamber.

3.3 Experimental setup

In this section the experimental setups of the μPIV and the 3D PIV are described. Even though the two setups are quite different, most of the equipment used is the same. It consists of high-speed cameras (Zyla 5.5 sCMOS USB 3.0, Andor, Oxford Instruments plc, Tubney Woods, Abingdon, UK) used with macro objectives (Laowa 100mm F2.8 CA-Dreamer Macro 2X, LAOWA, Weiden, Germany), a Nd:YAG laser - wavelength 532 nm - (Bernoulli 200-15, Litron Lasers Ltd, Rugby, Warwickshire, England). Both are connected to a synchroniser

(LaserPulse Synchronizer 610036, TSI Inc., Shoreview, MN, USA), which synchronises the camera shots with the laser pulses. To control the flow a syringe pump (LA-100, RS232, Landgraf Laborsysteme, Hannover, Germany) is used. Additionally, a inverted microscope (Olympus IX73, Tokyo, Japan) is used for the μPIV experiments. While for the 3D PIV a motor (Velmex VXM^{TM} , Velmex, Bloomfield, NY, USA) with a slide (BiSlide Positionong Slide, Velmex, Bloomfield, NY, USA) is needed. One big difference between the two setups is the used software. For the μPIV the 4G Insight software (4G Insight 11.1.0.5, TSI Inc., Shoreview, MN, USA) is used, while V3V Insight software (V3V Insight, TSI Inc., Shoreview, MN, USA) is used for the 3D PIV. Another difference are the tracer particles. The 2 μm Fluoro-Max red fluorescent polymer microspheres (Thermo Fisher ScientificTM, Waltham, MA, USA) and 5.03 μm PS-FluoRot-Partikel (Micro Particels GmbH, Berlin, Germany) are used for the μPIV while 55 μm polyamide particles (LaVision GmbH, Göttingen, Germany) are used for the 3D PIV. To adjust the graphs Tecplot 360 (Tecplot Inc., Bellevue, WA, USA) is used for the μPIV.

3.3.1 Micro PIV

Before the channels could be put into the test setup they needed some more preparation. Therefore, a microscope slide was glued onto the bottom side with the channel. A thin layer of superglue was added onto the flat surface. Than a microscope slide was put onto this layer, carefully in order not to clog the channel. In figure 3.29 a clogged channel can be seen. The red rectangle indicates an area, in which glue leaked into the channel. This can happen either when too much glue was put on the surface or when to much pressure was put onto the glass to press it down. But if too little glue was put on the surface the liquid could leak under the glass which would interfere with the flow during the experiments. After a few tries the right amount of glue was found. The make sure the glue was dried completely the channels were placed over night in a box with the microscope glass side up.

Prior to the start of the experiment thin paraffin stripes were added on the Luer connectors of the channel. This helped to prevent leakage during the experiment. Afterwards tubes with the counterpart of the Luer connector were screwed on. One tube leads to the syringe pump, the

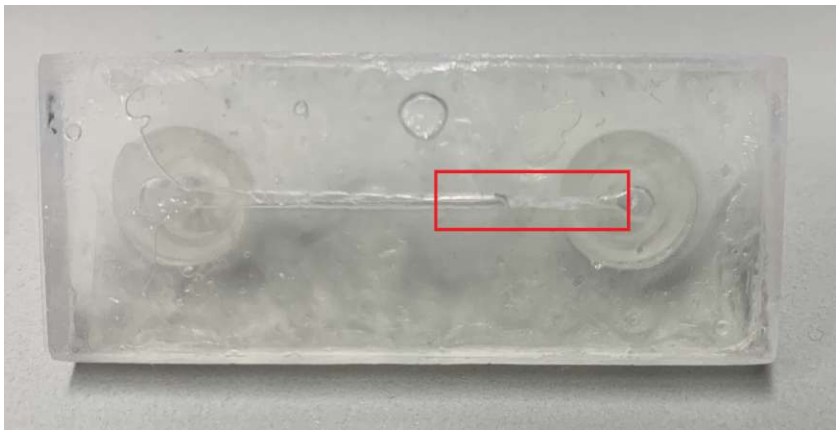

Figure 3.29: The red rectangle highlights the part of the channel, which got clogged with glue. This happened during the process of gluing the microscope slide onto the channel and not being careful enough.

other one to a second syringe, held by clamps. In figure 3.30 the placement of the specimen is shown in the setup, as well as the overall composition of the μPIV experiment. The laser light is redirected with a fibreglass tube, which is also connected to the microscope. Likewise, the camera used is directly connected with the microscope.

Once the channel was secured with tape on the microscope the fluid was pumped through the two tubes to ensure no leakage happened during the experiment. The first type of experimental liquid consists of water with 5 % tracer particles with a diameter of 2 μm. Therefore, this mixture was used multiple times. Before usage it was placed in an ultrasonic bath for 10 minutes, to separate the individual particles. With the 4x magnification of the microscope the structure inside the channel was inspected and a geometry was selected. But not all of them could be used because some of them collected small air bubbles, as seen in figure 3.31, which disturbed the flow. Afterwards, the magnification was switched to 10x and the ROI was defined, it will stay the same for the different velocities of one channel. This was all done with the light on an the PIV setting on free and the capture input was on continuous. When the experiment started this setting was switched to synchronised and a sequence of 100 pictures were selected. To avoid errors due to the ceiling light a cardboard box was placed over the sample.

Additionally, particles with a diameter of 5 μm were purchased. They were mixed with deionised water to get a concentration of 8 %. These particles were used with a 4x magnification. Typical ROIs are shown in figure 3.32, **A** shows the 10x with the 2 μm particle and **B** shows the 4x

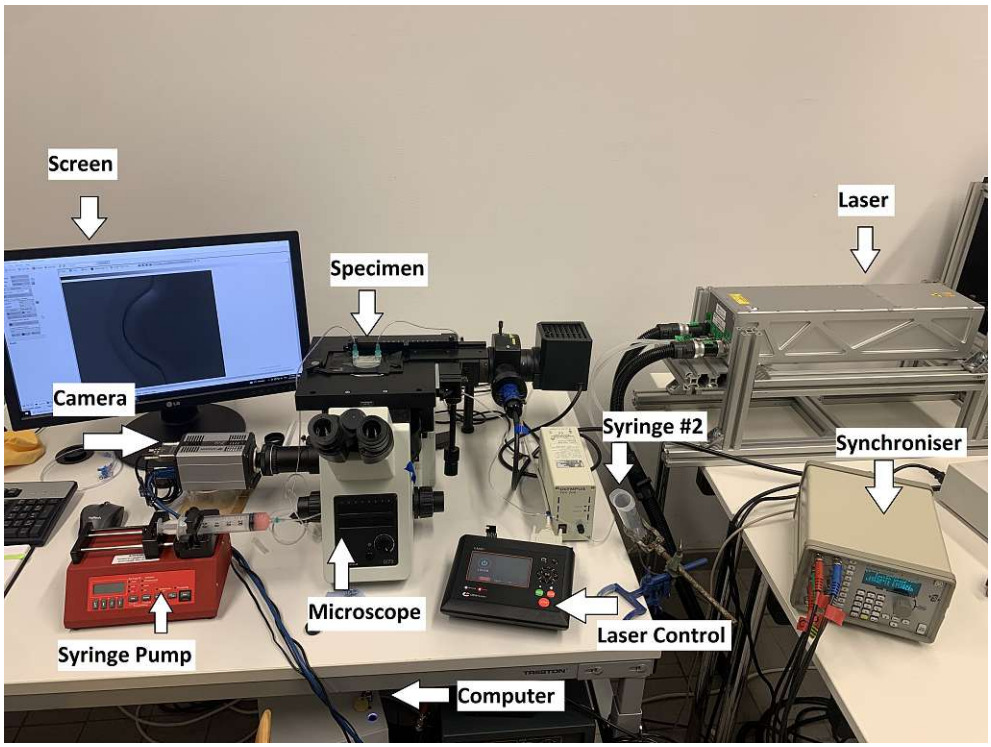

Figure 3.30: The experimental setup of for the micro PIV. With the computer for the software and the computer screen. The two syringes, one placed in the pump and the other one held by a clamp. The laser with its control board and the synchroniser. The microscope, with the mounted camera and the specimen placed on top.

magnification with 5 μm particles. The black part is the geometry while the light grey part shows the fluid with the particles inside.

Figure 3.31: An air bubble in the corner of the geometry in the channel. This bubble makes this specific ponit in the channel unusable if the bubble can not be removed.

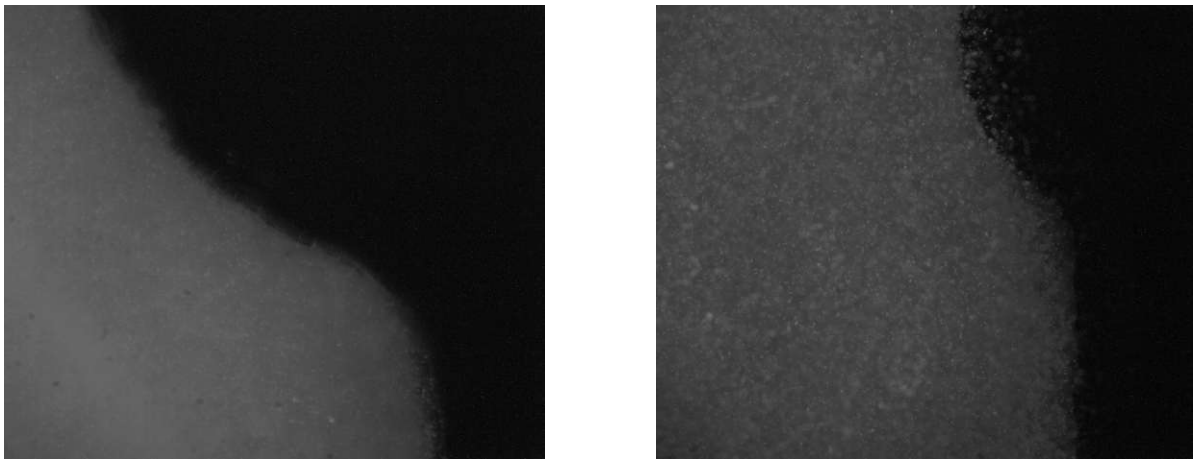

(a) 10x with 2 μm (b) 4x with 5 μm

Figure 3.32: The different ROIs at different magnifications. The black part shows the printed channel while the light grey shows the fluid with particles. The pictures were taken with the laser pulsing.

For the velocity inside the channel 0.5 mm/s, 1 mm/s and 1.5 mm/s were chosen. With the continuity equation and the equation for the flow rate the input for the syringe pump was calculated. To determine the correct ΔT a single shot was taken. With the help of the grid, provided by the software, the ΔT was chosen. The ΔT was modified until the particles travelled approximately one third of one rectangle of the grid. Table 3.4 shows the summary of the velocity, the input and the ΔT. This values were the same for every experiment with the μPIV. The flow was tested in two directions on the same ROI. The forward and back flow is illustrated in figure 3.33. The red arrow shows one direction and the green the other.

Table 3.1: Summary for the velocity, the input of the syringe pump with the corresponding ΔT for the μPIV.

velocity inside the channel	input syringe pump	delta T
0.5 mm/s	0.18 mL/min	25,000
1 mm/s	0.36 mL/min	18,000
1.5 mm/s	0.54 mL/min	11,000

Post processing with 4G and Tecplot

After capturing a series of 100 pictures the standard post processing, according to the handbook of the 4G software, was done. With the calibration the interrogation window was defined which

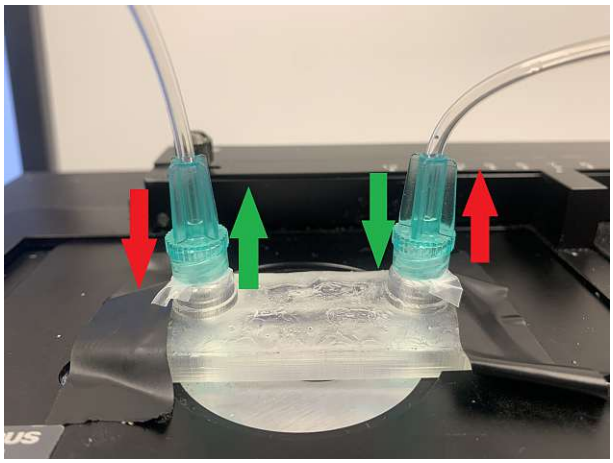

Figure 3.33: Close up of the micro PIV sample. The red and green arrows show the two different directions of the tested flow.

converted the pixels to mm. If the arrows created by the software showed a good statistic, meaning mainly green and yellow arrows, the data was opened by Tecplot. This is a built in software. The arrows were all manipulated to show a uniform appearance. The maximal values of the legend were all set to the same values for the three different velocities.

A final summary of the printed channels with the most important properties is listed in table 3.2.

Table 3.2: Summary of the printed channels for the μPIV.

Channel	Channel depth	Channel width	circle radius	additional info
C1	2 mm	3 mm	0.5 mm	the cylinder only touched the channel wall by a tangential point
C2	2 mm	3 mm	0.5 mm	the cylinder was shifted into the channel wall by 0.25 mm
C3	2 mm	3 mm	0.5 mm	the cylinder was shifted into the channel wall by 0.5 mm
C4	2 mm	3 mm	0.5 mm	the cylinder was tilted by 30 ° and shifted into the channel wall by 0.5 mm
C5	2 mm	3 mm	0.5 mm	the cylinder was tilted by 50 ° and shifted into the channel wall by 0.5 mm
C6	2 mm	3 mm	0.5 mm	the cylinder were tilted by 45 ° doublet -forming an X - and shifted into the channel wall by 0.5 mm

3.3.2 3D PIV

In figure 3.34 the experimental set up of the 3D PIV can be seen. Since space is limited the computer and monitor are further away as compared to the micro PIV. The Laser is pointed at the water tank, which stands on a small hoist. The calibration target - and later the sample - is mounted on a slide. Behind the tank is the light used for the calibration. The four cameras are mounted on tripods and all face the tank from the same direction. They are plugged into the synchroniser, just like in the μ-PIV set-up. To avoid unnecessary light pollution during the experiment the frame will be covered with black plastic plates.

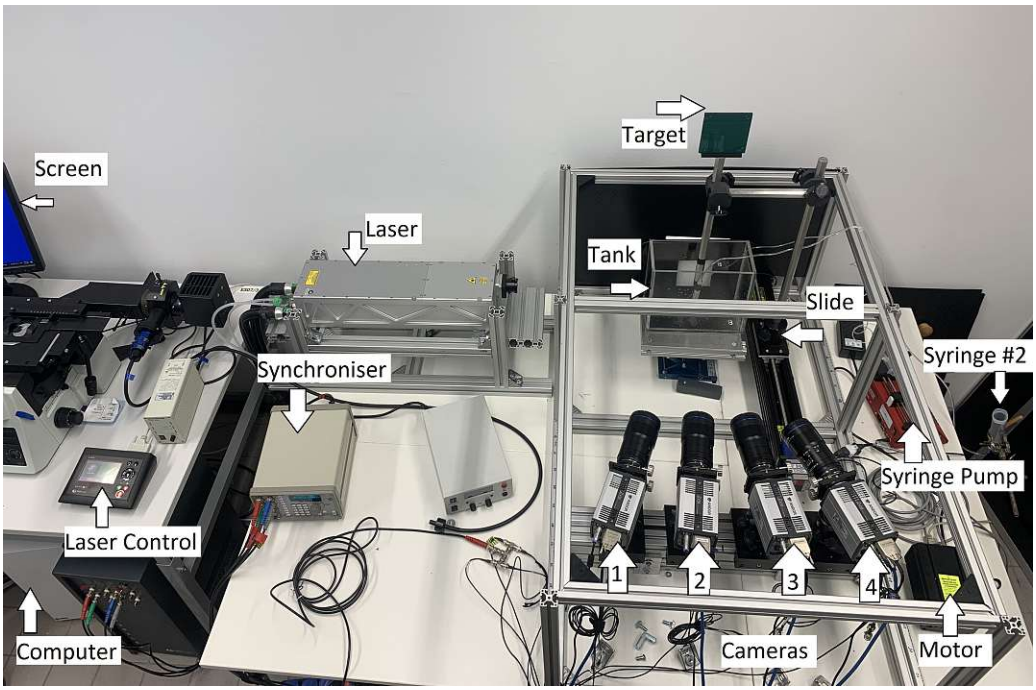

Figure 3.34: The setup of the 3D PIV. Showing the computer and screen, the laser with its control penal, the synchroniser connected to cameras 1 - 4. The target is mounted upside down so the sample can be in the tank, both mounted on the slide controlled by the motor. Syringe #1 is fixed into the syringe pump and syringe #2 is fixated on the table.

The number of cameras used for 3D PIV measurements requires a specific placement of all components. In the set up the best angle, which the outer two cameras enclose, is 90°. Therefore, the cameras were all placed with a spacing of 50 mm between each camera. The middle of the four cameras was placed in regard to the middle of the tank. The distance between the target in the water tank and the objective of the middle camera is 450 mm. For better understanding this placement is shown in figure 3.35.

Before the sample can be placed in the water tank the Luer connectors are connected to the

tubes leading to the syringes. Paraffin strips are placed on the connectors in the same way as it was done during the μ PIV tests. Water is then pumped through the sample to test if there are any leakage. After the water is removed again the sample is mounted with tape on the rode of the calibration target. This ensures, that the specimen sits in the middle of the calibrated ROI. The process of the calibration will be explained later. This can be seen in figure 3.36. Additionally, this figure indicates the direction the fluid will be pumped through the sample, specifically from bottom up. In syringe #2 additional fluid with particles was filled. After all the cavity was filled with fluid, the syringe pump was set to withdraw to fill syringe #1 as much as possible without getting air into the tubes again. This was done with all samples alike.

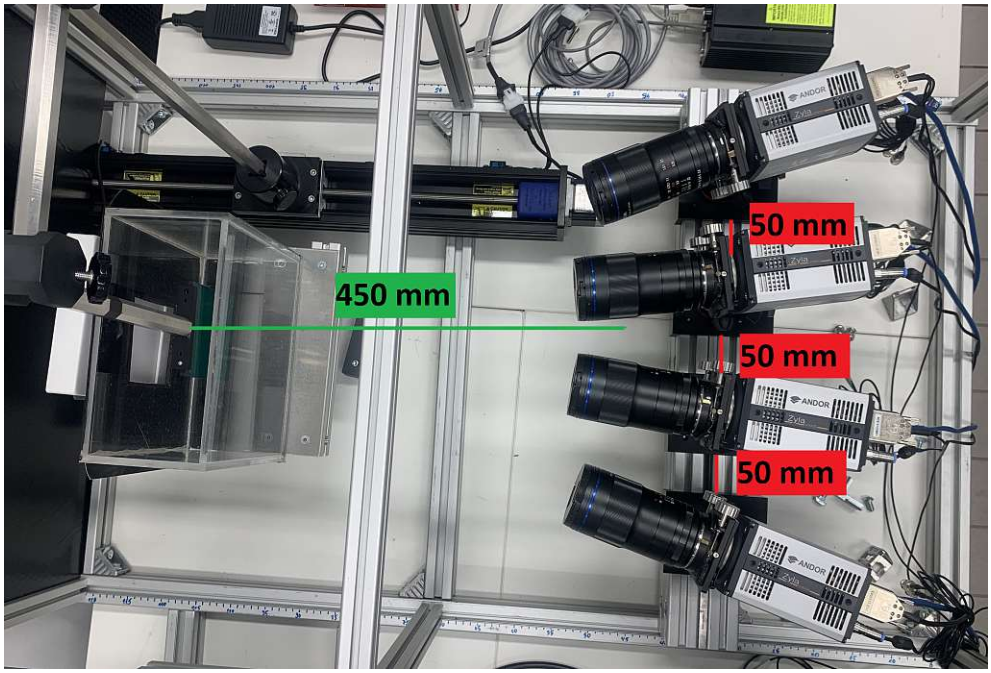

Figure 3.35: The camera set up viewed from above. The distance between each camera is 50 mm and from objective to tank it is 450 mm.

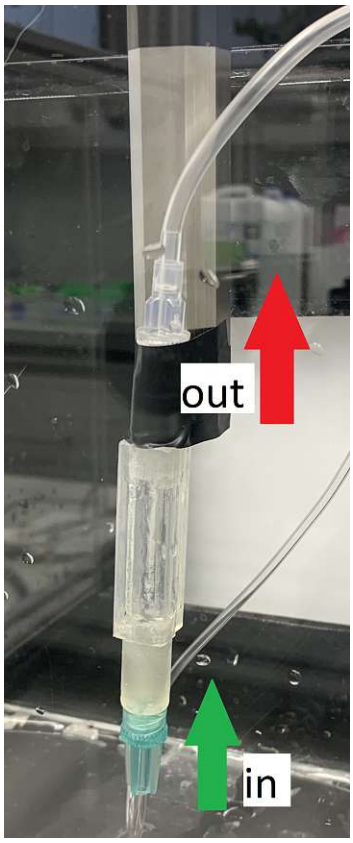

Figure 3.36: The sample is fixed to a rod and the test fluid is pumped from bottom to top, as indicated by the arrows.

For the 3D PIV experiments the same velocities chosen during the μ-PIV measurements were used. The flow rate of the syringe pump was adjusted according to the new diameter of the channel. These changes are summarised in table 3.3. The ΔT was also adjusted. Therefore pictures were taken and the values were changed until satisfaction. Additionally, different lenses were put on the laser to change the focal point and distribute the light in a better way.
For the particles a separate solution of 80 mL of 50/50 H_2O and glycerin was mixed and a teespoon of polyamide particles was mixed in. This solution was added step by step to another 80 mL of a 50/50 mixture. Until the particle concentration in the cameras looked similar to the one in the μPIV test. In the end, 8 mL were added and used for the testing solution.

Refractive Index Matching

In figure 3.37 the difference of visibility of the cylinder, without a clear coat, in a perceptual change in a mixture of water (H_2O) and glycerin can be seen. The same cylinder is placed in 3.37a the structure is placed in 100 % H_2O, it is clearly distinguishable. For the second mixture

Table 3.3: Summary of the velocity, the input of the syringe pump with the corresponding ΔT for 3D PIV.

velocity inside the channel	input syringe pump	delta T
0.5 mm/s	2.36 mL/min	2,000
1 mm/s	4.71 mL/min	1,300
1.5 mm/s	7.07 mL/min	600

Table 3.4: Summary of the geometries from the produced channels for the 3D PIV.

Cylinder	Material	Helix	additional info
H1	Silicon	no helix uneven walls	the form was too sticky and could not be demolded properly
H2	Clear resin	no helix	the thickness of the cylinder is 0.6 mm, the Luer Connectors got glued on
H3	clear resin	0.5 mm radius	the thickness of the cylinder is 0.6 mm, there are 3 full turns of the helix, the Luer Connectors got glued on
H4	clear resin	0.5 mm radius	the thickness of the cylinder is 0.6 mm, there are 3 full turns of the helix, the Luer Connectors and cylinder got printed as one piece

50 % of both H_2O and glycerin is used. The structure is clearer but is still very visible. In the last picture 3.37c 100 % glycerin were used. The helix inside is not visible but the edge of the cylinder are noticeable. Additionally, glycerin has a much higher viscosity than water and a higher density. This lead to two different observations. The 50/50 mixture was separated into tow phases until it was mixed well. The structure stared to float when placed in the pure glycerin. In figure 3.38 a cylinder with a clear coat is placed in either 3.38a - 100 % H_2O, 3.38b - 50 % of both H_2O and glycerin, or in 3.38c - 100 % glycerin.

Calibration

For the calibration a special calibration target, see figure 3.39, is used. This target is illuminated from behind and has three dark spots, which indicate the middle and help the software recognise

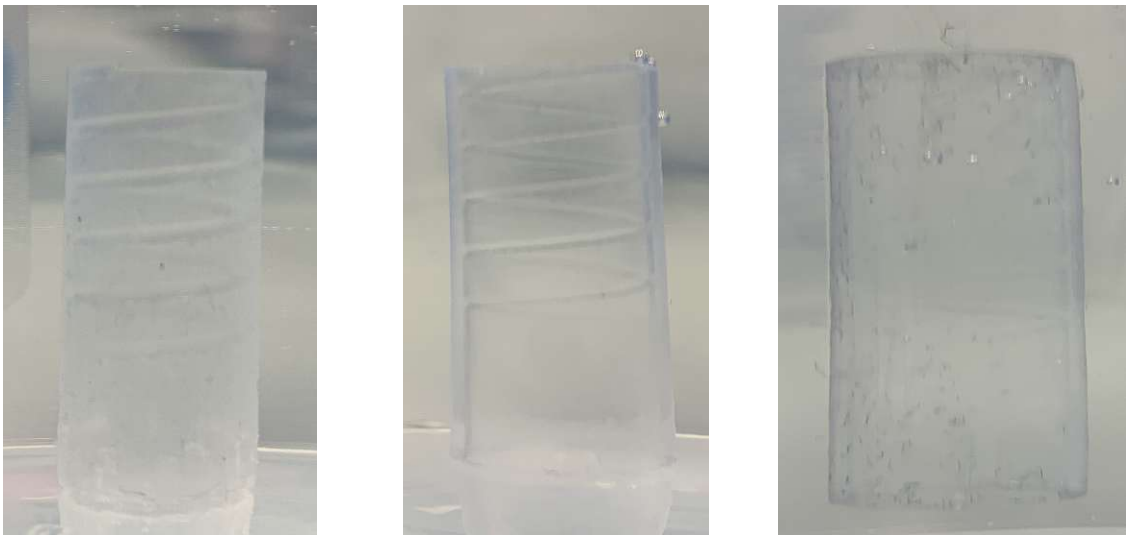

(a) 100 % H_2O (b) 50 % H_2O + 50 % glycerin (c) 100 % glycerin

Figure 3.37: The same printed cylinder, without post processing, is placed in different mixtures of H_2O and glycerin. Starting with 100 % H_2O, then 50 % H_2O and 50 % glycerin and at last 100 % glycerin.

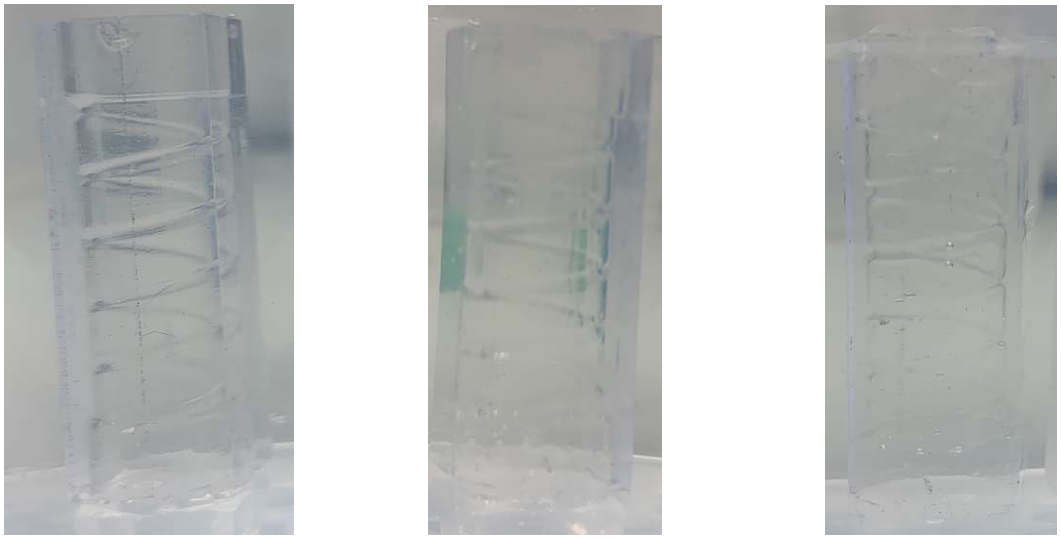

(a) 100 % H_2O (b) 50 % H_2O + 50 % glycerin (c) 100 % glycerin

Figure 3.38: The same printed cylinder, with post processing, is placed in different mixtures of H_2O and glycerin. Starting with 100 % H_2O, then 50 % H_2O and 50 % glycerin and at last 100 % glycerin.

the orientation. It is placed into the mount on the slide. The software is opened and with the free and 'continues' setting each camera is manipulated until the cross-hair is in the middle of the calibration target. Additionally, with the objective and the Scheimpflug adapter, all points are put in focus. this is especially important for the outer two cameras. When this step is done, the aperture is closed completely and the procedure is continued with the next camera. Once all the cameras are adjusted, the ROI is determined. The calibration target gets moved

back, half the length of the ROI. Now the calibration can be started.

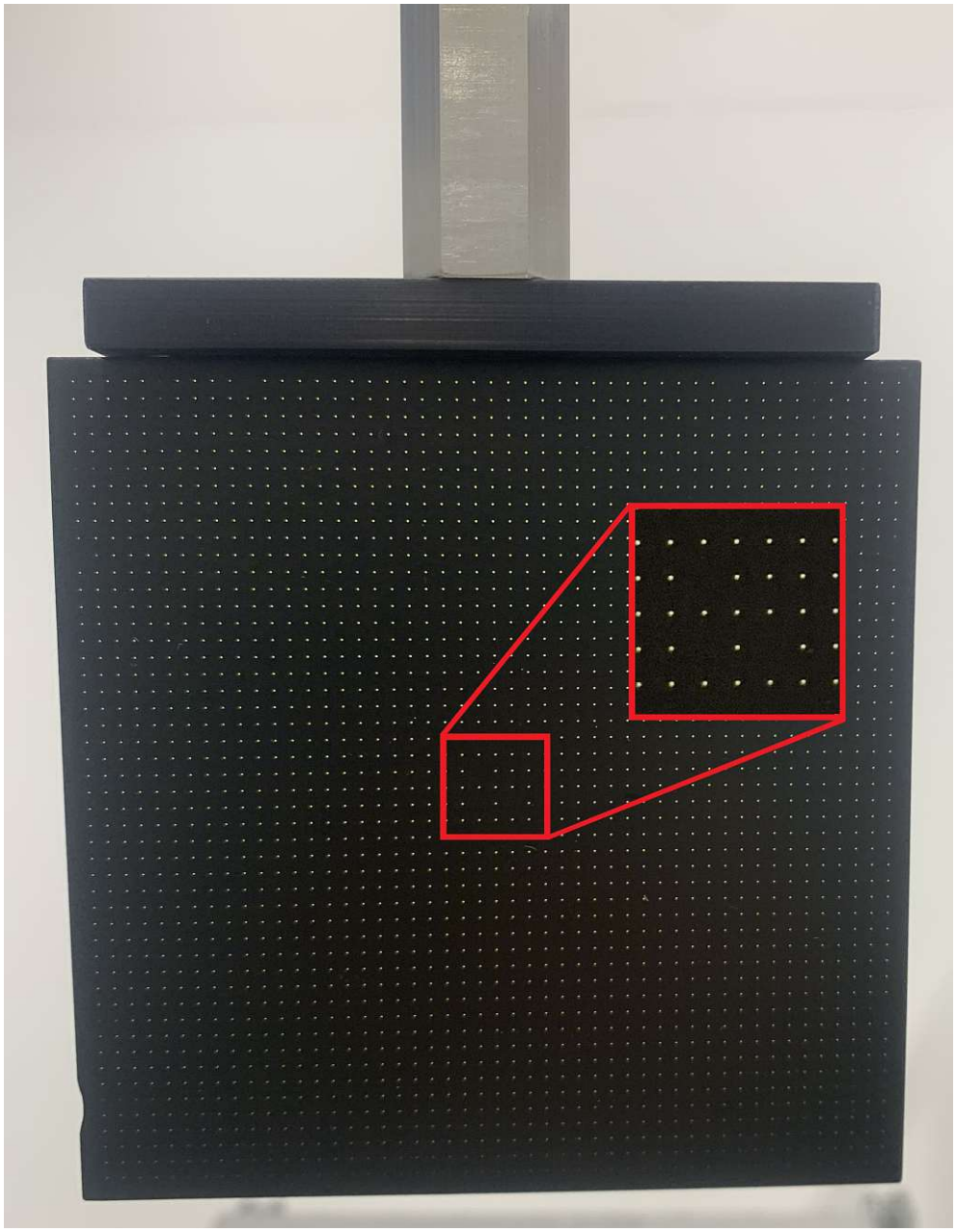

Figure 3.39: Calibration target for the 3D PIV. The red rectangle marks the middle of the target, which are the three dark spots.

4 Results

In this chapter, all the results generated during the experiments are summarised.

4.1 Micro PIV

The results for the micro PIV will be split into two. The two groups discussed will be Channels C1 - C3 and C4 - C6.

4.1.1 Experimental Results For Channels C1-C3

First the results from the measurements with the 10x magnification an 2 μm particles will be discussed. Afterwards the results recorded with the 4x magnification and 5 μm particles are shown.

10x magnification

The results are grouped by channel design. In all figures **(a)** and **(b)** show the results for the 0.5 mm/s input, **(c)** and **(d)** for 1 mm/s and **(e)** and **(f)** show the results for 1.5 mm/s. Furthermore the left-hand side showes the back movement of the fluid, while the right-hand side shows the forward motion. The mask used for the post processing is always the same for the same channel.

Channel C1 is displayed in figure 4.1. The velocity is very low for all of the three input values. The pointing direction of the arrows near the geometry, green circle in figure 4.1a, is in all 6 pictures similar random. More exact the area from -0.6 mm to - 0.45 mm in Y direction and 0.4 mm to 0.7 mm in X direction.

Channel C2 is displayed in figure 4.2. The velocity profile is uniform in all 6 pictures. The back movement shows a little more turbulence around the edge of the geometry, green circle in figure 4.2a. This area is at -0.5 mm to -0.45 mm in Y direction and 0.4 mm to 0.6 mm in X direction.

Channel C3 is displayed in figure 4.3. The velocity is higher near the middle of the channel and the flow profile is more uniform than in the channels before. The difference between the forward and the back flow is more visible around the geometry, green circle in figure 4.3a.

Comparison of C1 - C2 - C3 shows that the flow gets more linear when the structure is half embedded into the structure wall. The turbulence near the wall and in the nook also decreases significantly.

4x Magnification

The weight of the 5 μm particles made it impossible to test the channels with the velocities chosen. In figure 4.4 the shadow cast by the particles not in focus can be seen. This lead to no usable results, the arrows processed by the software pointed in every direction. Therefore no flow profile was generated and the values were near zero. Additionally, the particles started to stick on the glass cover after the first test. This can be seen in figure 4.5, the lighter middle part are particles sticking to the glass. This again lead to no result.

4.1.2 Experimental Results For Channels C4-C6

The focus was near the glass surface during testing, which was needless for this channels, as the interesting geometric structure is in the middle of the channel. If the focus was in the middle

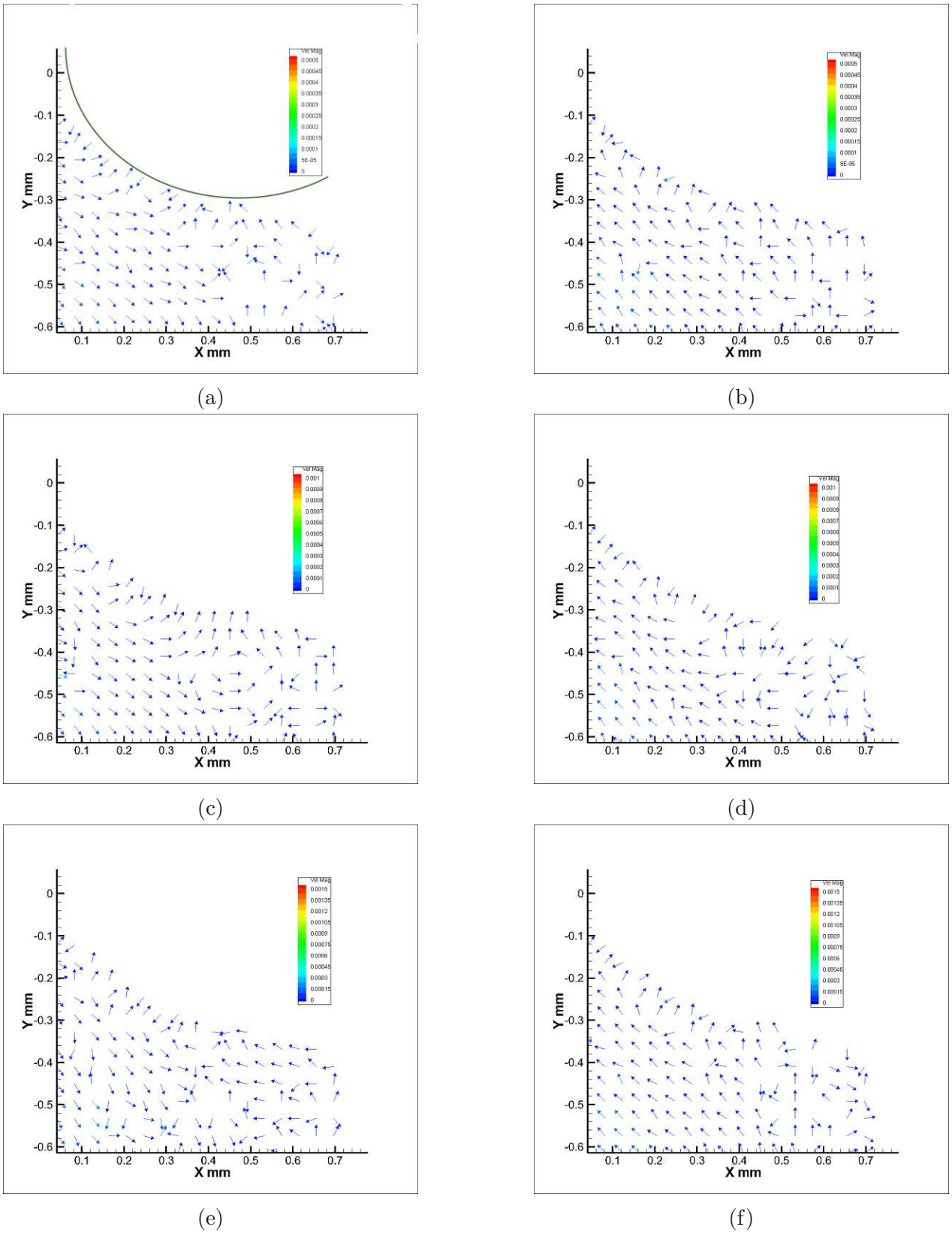

(a) (b)

(c) (d)

(e) (f)

Figure 4.1: The different plots generated for 0.5 mm/s - a and b - for 1 mm/s - c and d - and for 1.5 mm/s - e and f. In the back flow, left hand-side and forward flow, right hand-side for Channel C1. The geometry is indicated in the first picture as a green circle.

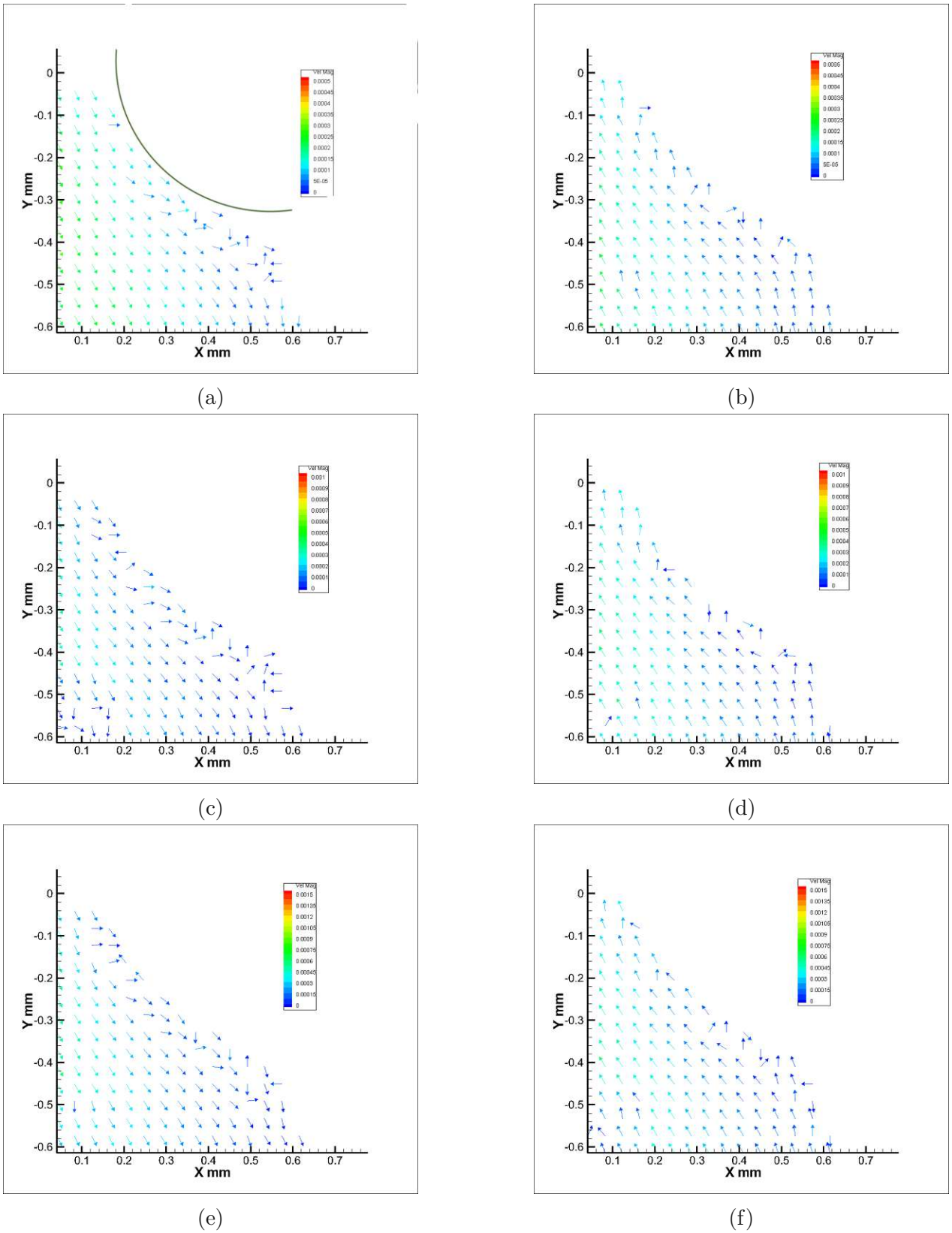

(a) (b)

(c) (d)

(e) (f)

Figure 4.2: The different plots generated for 0.5 mm/s - a and b - for 1 mm/s - c and d - and for 1.5 mm/s - e and f. In the back flow, left hand-side and forward flow, right hand-side for Channel C2. The geometry is indicated in the first picture as a green circle.

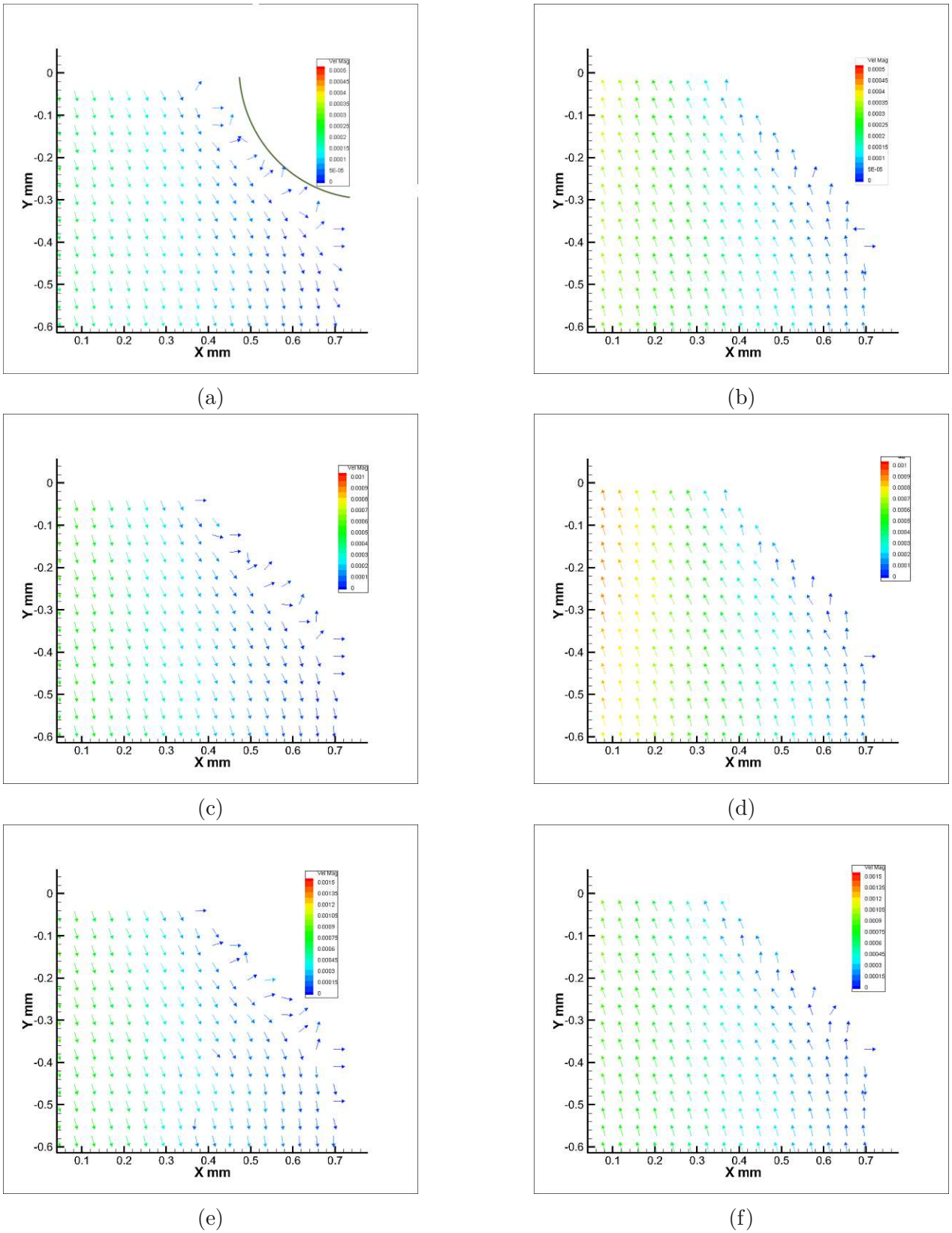

Figure 4.3: The different plots generated for 0.5 mm/s - a and b - for 1 mm/s - c and d - and for 1.5 mm/s - e and f. In the back flow, left hand-side and forward flow, right hand-side for Channel C3. The geometry is indicated in the first picture as a green circle.

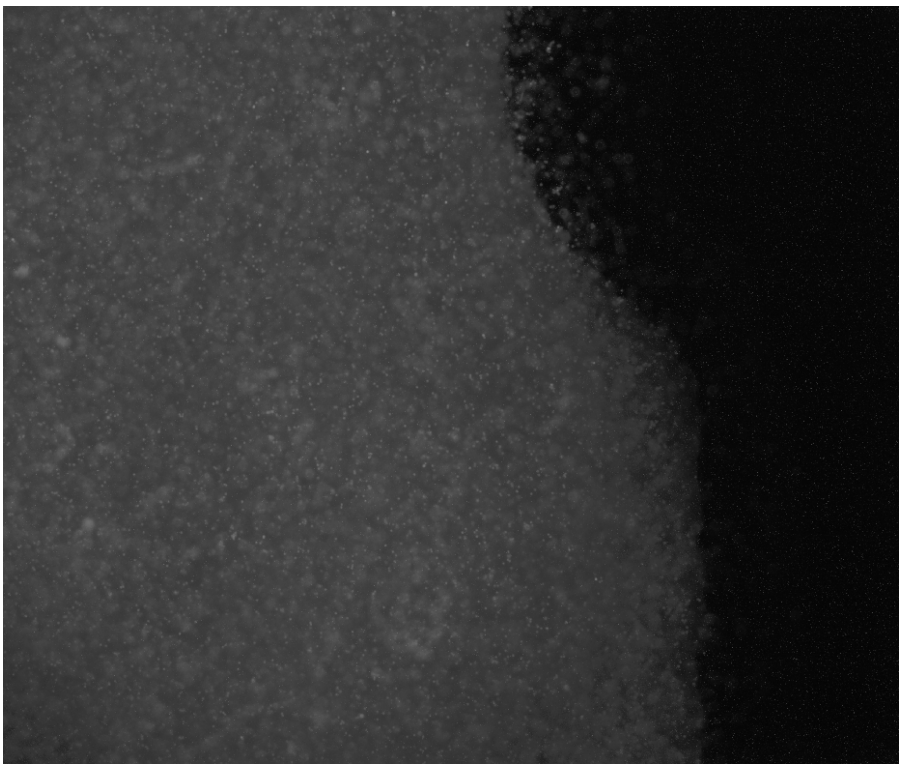

Figure 4.4: Particle shadows in the channel with a 4x magnification.

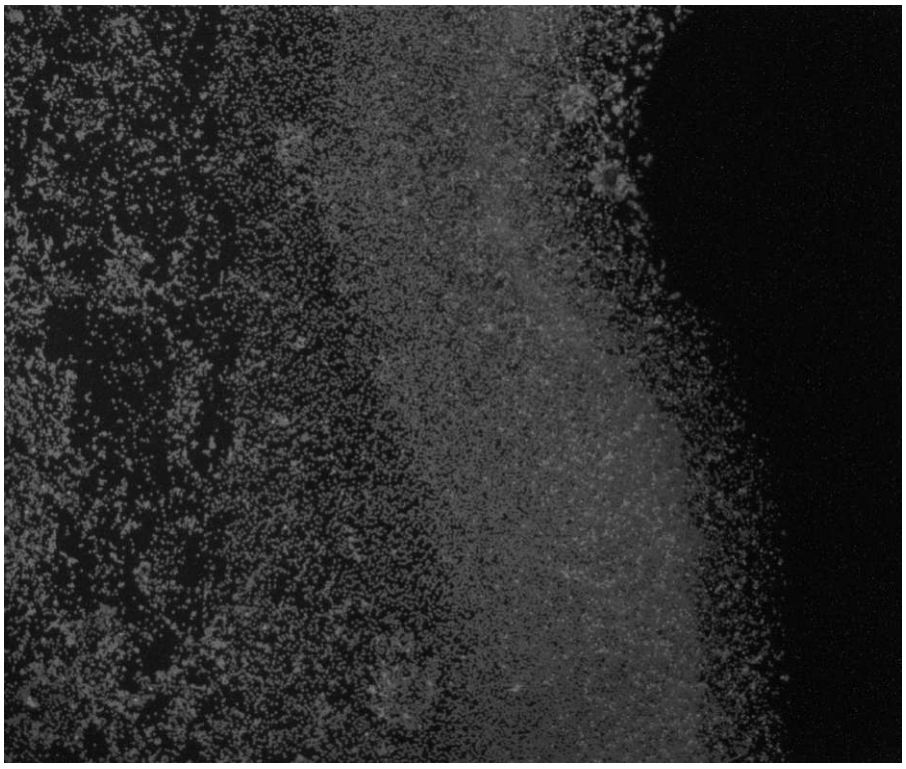

Figure 4.5: Particles sticking to the glass, light grey area, after flushing the channel with water.

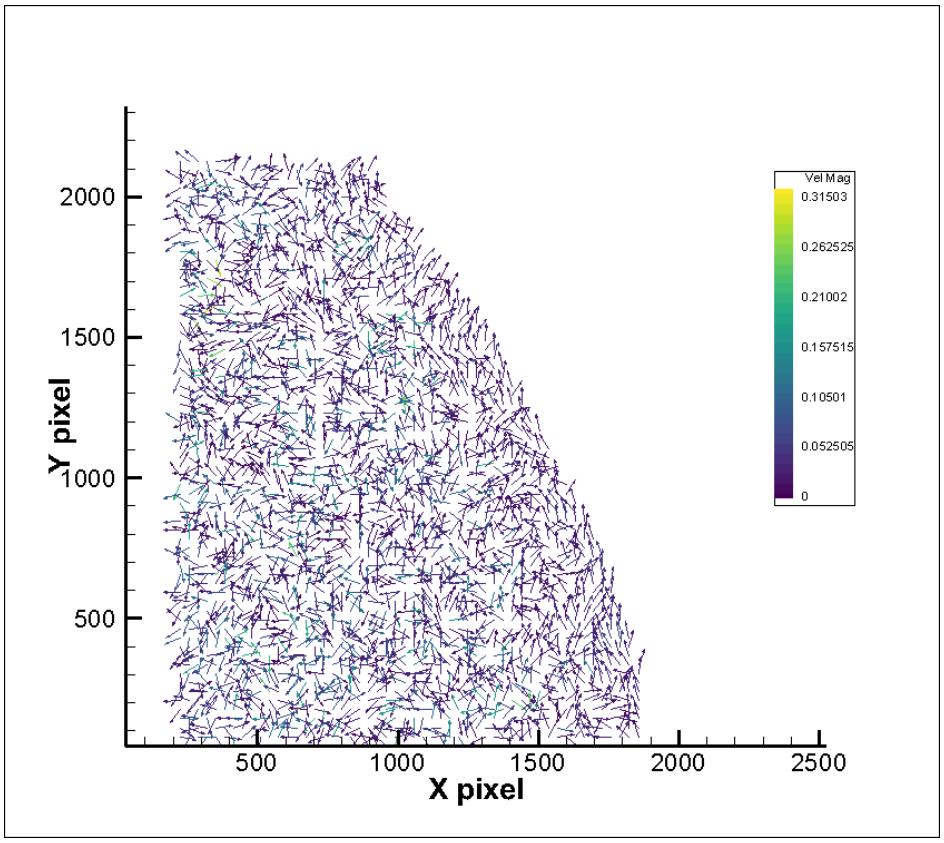

Figure 4.6: An example of a bad plot for the micro PIV. The arrows are pointing in every direction and have a value of nearly 0.

of the channel the shadows of the the particles not in focus were too much for the program. It could no longer follow the individual particles and therefore no results were possible. The arrows generated after post processing did not show any flow profile. The values were very low and the arrows pointed in every direction. Figure 4.6 shows an example of the generated vector plot.

4.2 3D PIV

At first the results of the calibration are shown, then the difference the lens on the laser makes and lastly the qualitative results of the measurements are displayed. For the measurements only cylinder H3 is used.

4.2.1 Calibration

One very important result for the 3D PIV measurements is the calibration statistic. This statistic can be seen in figure 4.7. The four cameras are each represented by a different color. From camera #1 to camera #4 the order is as following, left (green), right (red), top (blue) and bottom (yellow). The *aperture-specific origin location* shows the way of the mark in each frame. Meaning that the movement, relative to the camera, of the center of the calibration target is mapped in this plot. A straight line shows, that the way was smooth. The four graphs on the left show different important plots. On the top the ***nominal magnification*** for every level is seen. Then the world to camera ***error in pix***, comparing the error between actual and computed 2D image. The camera to world ***error in micron***, compares the error between the actual and computed 3D image. Both of these values are small in the generated calibration. The last plot shows the number of valid ***grid points*** found in each image.

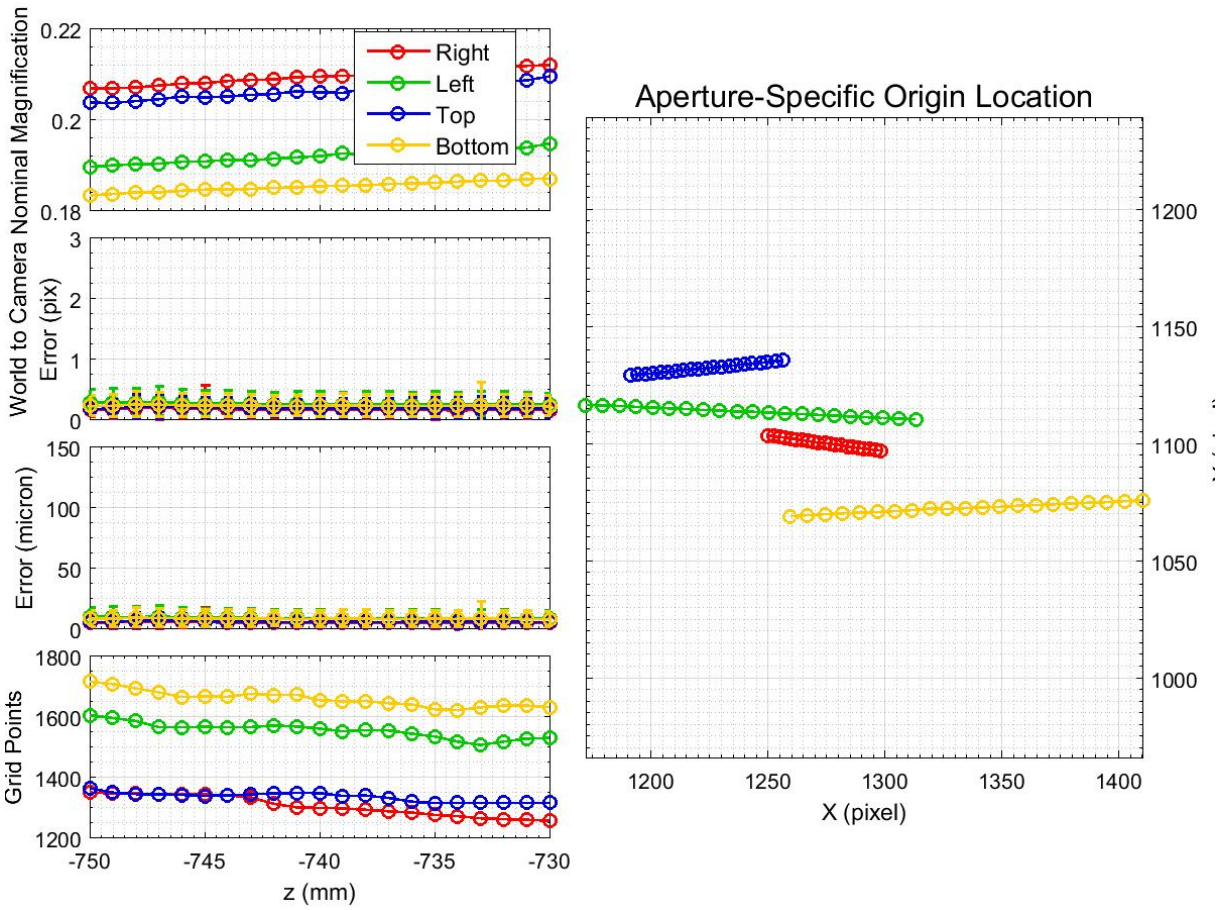

Figure 4.7: The calibration statistic generated by the V3V software.

In figure 4.8 the plot of the reconstructed grid points is shown. Most of the points are aligned,

but as it can be seen, there are some that look like, as if they were not on the right place. Two other tests made to determine if the calibration is valid or not was the yield in particle matching in the processor output window. If its higher than 85% the calibration is valid. Secondly, the XY view of the dot plot was chosen, and again there were no outlier.

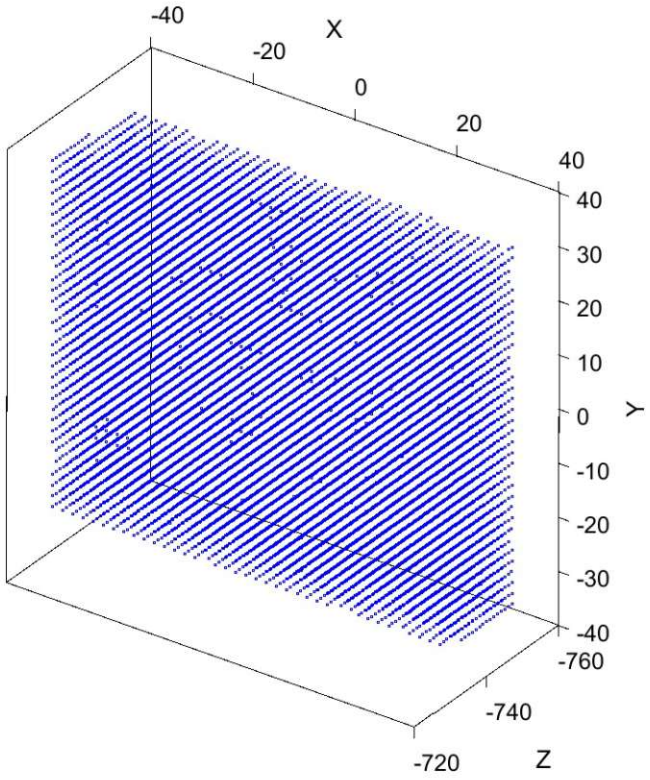

Figure 4.8: The calibration dot plot generated by the V3V software.

In figure 4.9 the difference between no lens 4.9a, a 25 μm lens 4.9b and a 50 μm lens 4.9c can be seen. The hot pink spots on in the pictures indicate an overexposure. With no lens there is a local overexposure in the bottom of the channel. The 25 and 50 lenses both show a better distribution of light, where the 50 μm shows more pink spots in the channel itself.

In figure 4.10 the mask used during the post processing can be seen, the red rectangular. It only includes the part of the cylinder with the helix inside. In figure 4.11 the plots of the three different velocities can be seen. Starting at the top with 0.5 mm/s, 1 mm/s and 1.5 mm/s input velocity. The plot is sliced on the Y axis and once in the X axis, to show the middle of the channel. It can be seen in each slice, that there could be no velocity measured. The pink arrows indicating the velocity direction are pointing in every direction.

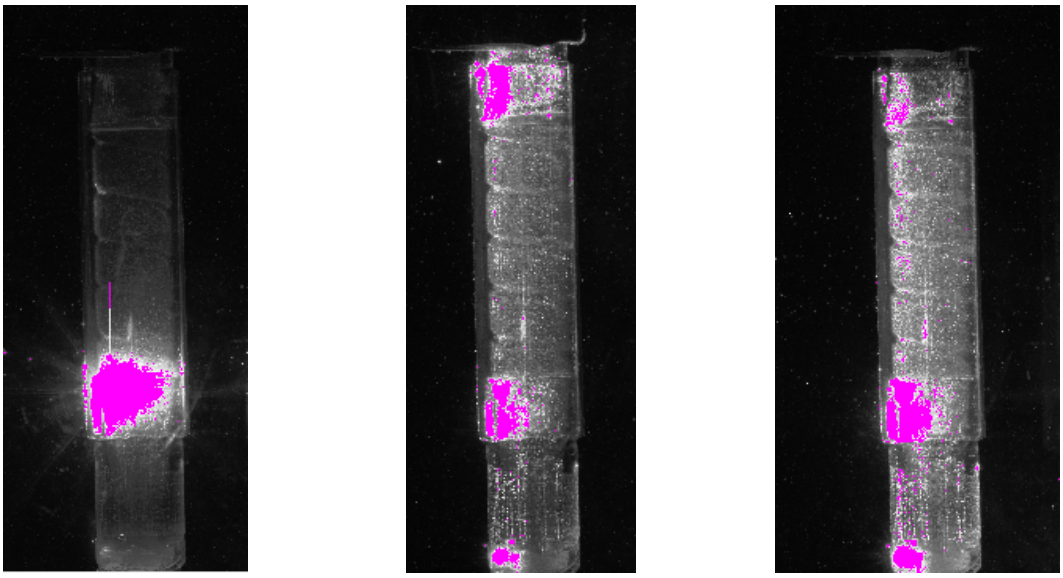

(a) (b) (c)

Figure 4.9: A comparison of different lenses put onto the laser. In 4.9a no lens is added. In 4.9b a 25 μm lens is added. In 4.9c a 50 μm lens is added. The hot pink shows overexposure.

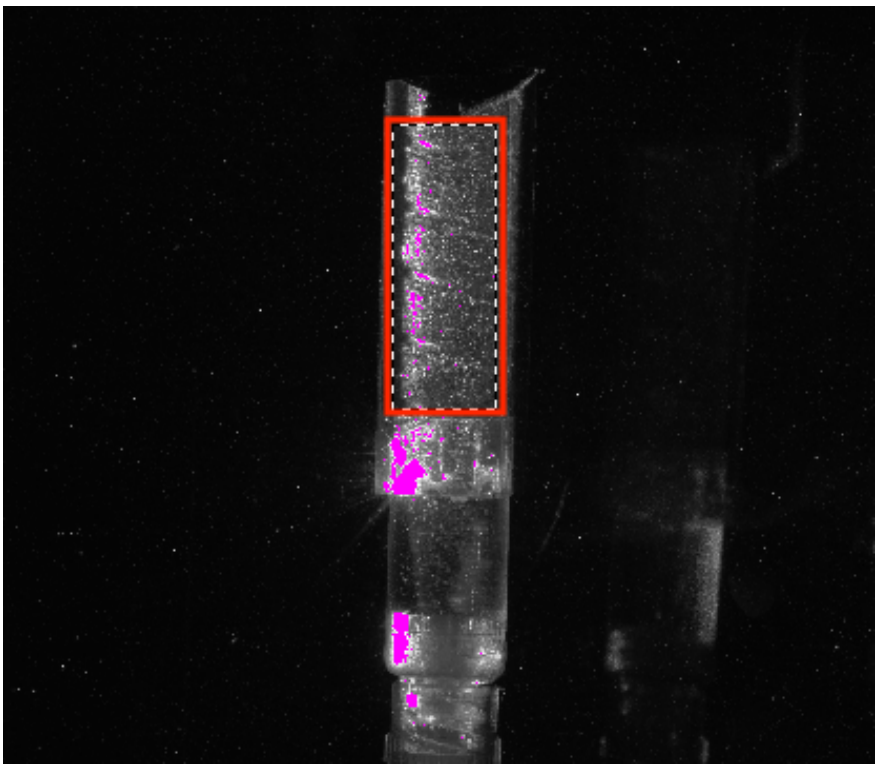

Figure 4.10: The red rectangular shows the mask used for post processing during the 3D PIV measurements.

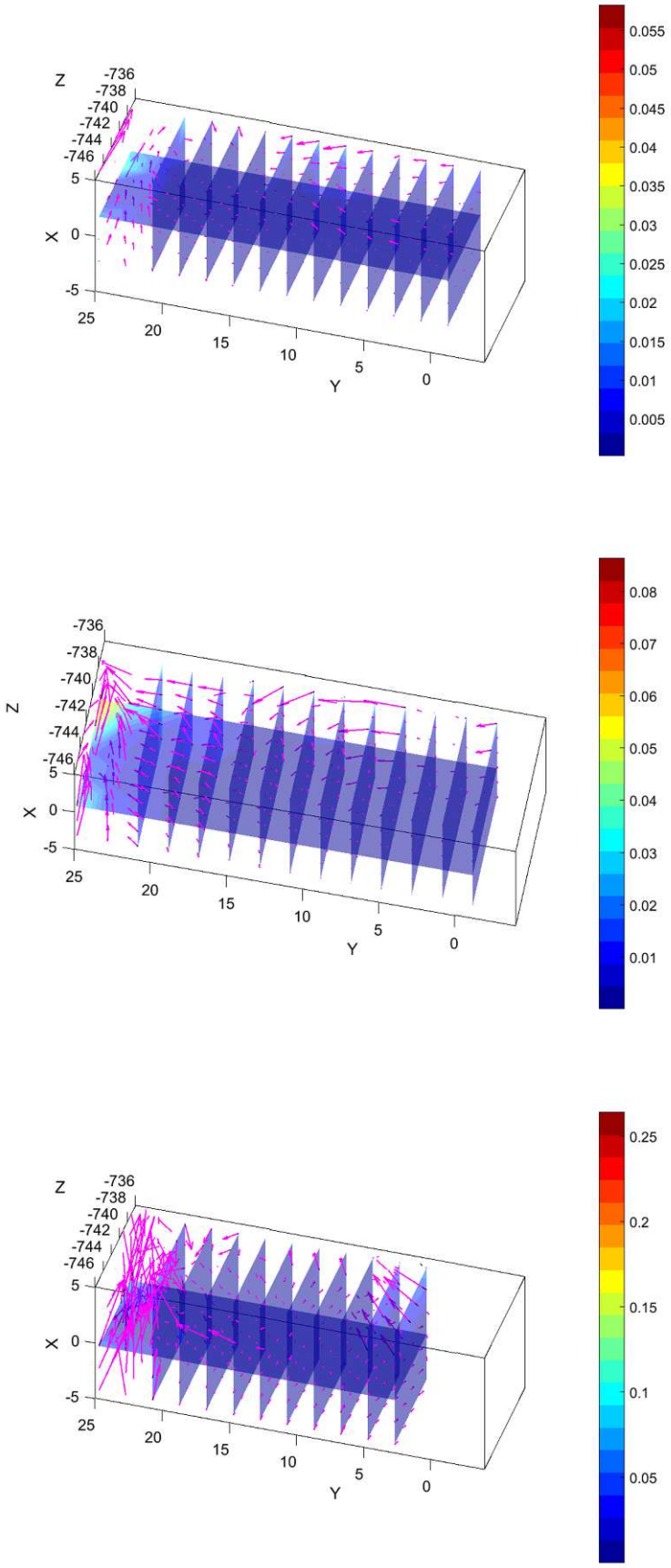

Figure 4.11: The velocity profiles of the 3D results. From top to bottom 0.5 mm/s, 1 mm/s and 1.5 mm/s input velocity. It only shows the area of the masked part.

5 Discussion

In this chapter the results will be compared to other papers and will be discussed critically. Furthermore some problems which had to be faced during the experiments will be reviewed. The aim of the thesis was to compare different obstacles in a channel with a 3D PIV and μPIV system and lern where the dead space and slow flow occurs. The results from the μPIV are as expected. For the 3D PIV a different approach for the samples is needed. All the details for this outcome are discussed in this chapter.

5.1 Comparison

In the study from Melzer et.al. (2019) [45] the flow characteristics before and after a round obstacle, show the same behavior as the one observed in the micro PIV experiments in this thesis. The flow after the stent shows more turbulence and a higher dead space. This would lead to more clumping of the plates after insertion of the stent.

Additionally, the geometry difference between the three channels leads to the same result as it is observed in medicine. The highest risk for patients occurs in the first half year after stent implantation. [25] The dead-space and slow flow profile near the walls helps plates to stay there longer and begin to clump.

Unfortunately, no comparison between the 3D and the micro PIV data could be made, as the 3D plots show no velocity field.

5.2 Complication During The Experiments

In this section some complications arising during the manufacture of the samples and during the measurements will be discussed.

5.2.1 Micro PIV

Printing

The printing of the channels was not that easy as they had to be adjusted to the limitations of the printer. A comparison between geometries with more or less space in between the individual circles was not possible, as the printer simply could not print the structure. The addition of the support structures also seem to really influence the quality of the print, if too few were used, in order to not damage the Luer Connector during the post processing too much, the printer would not print them at all. If the channels fell off of the printing plate the whole resin hat to be filtered, as small hardened particles in the resin would have a bad influence on the quality of the print.

Also the resolution of the printer appeared to get worse over time. During the printing not every channel was printed properly even though the support structures were the same and the parts were printed simultaneously. The individual layers were also visible with the naked eye. This also is not ideal for the experiments. Supplementary, Kleedorfer [37] came to the result, that the newer generation of the printer showed better results.

Measurements

The preparation of the channels before measuring had to be done carefully. The microscope slide either did not stick to the channel well enough, if to little glue was used, or the glue was spilling into the channel. This was both not beneficial for the experiments. In the first case the particles would wander under the glass plate and the mask had to be chosen more carefully. In the second case the channel could not be used, as the super glue will get opaque when in contact with water or a shadow is seen in the images.

The only channels that could be measured were the ones with only straight cylinders. The ROI

for the others was in the area in which the particle shadows interfere to much with the picture. If the channels could be made less deep the channels with other geometries could be tested as well. The problem with the geometries in the middle is linked to the depth of correlation. [46] [47]

5.2.2 3D PIV

Printed cylinder

It turned out that the printing of the cylinders was more difficult than expected. The support structures had to be added carefully to not sit on the geometry part of the cylinder, if too little support was chosen the print would just fall of the printing plate. The layers of the printer were very visible and even after adjusting the design and post processing it in a similar way as Stanley et.al. (2023) [42] the same transparency was not achieved. Furthermore, the surface got shiny and reflected the laser light which lead to a uneven illumination of the channel during the experiments.

The plots show no velocity field, which can be due too the low transparency of the cylinder. The particles could be seen on the images, when looked on the computer screen during the investigated the images. It could also be, that the particles sunk due to a low input flow.

Silicon form demolding

It was not possible to make a silicon form usable for the measurements. The silicon was too sticky even though the ratio of the two components was adjusted. When the plates were removed the form stuck so tight onto the metal that the form was destroyed. Additionally, the wax could not melt completely and some small parts still were left in the form. After hot water was used to flush the channel the silicon turned opaque.

6 Conclusion And Outlook

The aim of this thesis was to investigate the behaviour of the blood flow in a blood vessel with an obstacle. Therefore, channels were designed to mimic the flow. The results of both 3D PIV and e μ-PIV were gathered and compared.
In conclusion, even though the samples for the μPIV were not ideal a quantitative result of the experiments showed similar flow outcomes to the ones found in literature. [45] Therefore, we gained the understanding, that the flow is more disturbed after the obstacle and that the shape should be a drop shape to show a better flow profile.

Particle image velocimetry is a highly sensitive system and needs the most transparent test samples possible without reflecting the laser light. Therefore, some suggestions for a further sample optimisation are made in the next paragraphs.

To get even better results prints with a better printer could be made, for both 3D and micro PIV. Additionally, the RI could be matched even more closely, for more transparency. With a different setup the fluid cloud be pumped from another direction.

For the silicon mold a Teflon form could be a smarter choice for the form and a different silicon could be considered. Schult et. al. (2018) [48] were successful in manufacturing blood vessel dummies made from Elastosil®RT 601 (Wacker Chemie AG, Munich, Germany). While Yousif et. al. (2009) [49] used Sylgard 184 (Dow Corning, Hoek, The Netherlands).

List of Figures

List of Tables

Bibliography

[1] World Health Organization. *Ageing and health*. 2021. URL: https://www.who.int/news-room/fact-sheets/detail/ageing-and-health.

[2] World Health Organization. *Cardiovascular diseases (CVDs)*. 2021. URL: https://www.who.int/news-room/fact-sheets/detail/cardiovascular-diseases-(cvds).

[3] A.H. Gershlick and R.K. Aggarwal. "Stent thrombosis revisited". In: *European Heart Journal* 17 (1996), pp. 1623–1628.

[4] Hiromasa Otake. *Stent edge restenosis -an inevitable drawback of stenting?* 2021. DOI: 10.1253/circj.CJ-21-0581.

[5] J. Fanghänel et al. "2. Allgemeine Anatomie". In: *Anatomie des Menschen*. 17th ed. Berlin: Walter de Gruyter, 2003, pp. 15–112. ISBN: 3-11-016561-9.

[6] Institute for Quality and Germany) Efficiency in Health Care (IQWiG. *How does the blood circulatory system work?* URL: https://www.informedhealth.org/how-does-the-blood-circulatory-system-work.html.

[7] Robert F Schmidt, Florian Lang, and Manfred Heckmann, eds. *Pysiologie des Menschen*. 31. Springer Berlin Heidelberg, 2011, p. 979. DOI: https://doi.org/10.1007/978-3-642-01651-6. URL: https://www.ptonline.com/articles/how-to-get-better-mfi-results.

[8] J. Fanghänel et al. *Anatomie des Menschen*. 17. Berlin: Walter de Gruyter, 2003. ISBN: 3-11-016561-9.

[9] Alistair Farley, Charles Hendry, and Ella McLafferty. "Blood components". In: *Nursing Standard* 27.13 (2012), pp. 35–42. ISSN: 0029-6570. DOI: 10.7748/ns2012.11.27.13.35.c9449.

[10] Russell Ross. *CELL BIOLOGY OF ATHEROSCLEROSIS*. Tech. rep. 1995, pp. 791–804. URL: www.annualreviews.org.

[11] Peter Libby. *The changing landscape of atherosclerosis*. Apr. 2021. DOI: 10.1038/s41586-021-03392-8.

[12] Peter Libby, Paul M. Ridker, and Attilio Maseri. "Inflammation and atherosclerosis". In: *Circulation* 105.9 (Mar. 2002), pp. 1135–1143. ISSN: 00097322. DOI: 10.1161/hc0902.104353.

[13] Peter Libby. "ATHEROSCLEROSIS: THE NEW VIEW". In: 286.5 (2002), pp. 46–55. DOI: 10.2307/26059682.

[14] Micah Girotti. *Atherosclerosis – a "Hard" Problem to Treat*. URL: https://www.vascularsurgeryass net/blog/atherosclerosis-a-hard-problem-to-treat.

[15] Mushabbar Syed and Michael Lesch. *Coronary Artery Aneurysm: A Review*. Tech. rep. 1997.

[16] Matthew A. Corriere and Raul J. Guzman. "True and false aneurysms of the femoral artery". In: *Seminars in Vascular Surgery* 18.4 (2005), pp. 216–223. ISSN: 08957967. DOI: 10.1053/j.semvascsurg.2005.09.008.

[17] R. J. Baird et al. "The false aneurysm". In: *Canadian Journal Of Surgery* 91 (1964).

[18] Malte Ludwig, Johannes Rieger, and Volker Ruppert. " 1.7 Arterielle Aneurysmen". In: *Gefäßmedizin in Klinik und Praxis*. Stuttgart: Thieme, 2010.

[19] Timothy A M Chuter. *Stent-graft design: the good, the bad and the ugly*. Tech. rep. 1. 2002, pp. 7–13. URL: www.elsevier.com/locate/cardiosurPH:S0967%C2%B72109.

[20] Anthony Lamanna et al. *Carotid artery stenting: Current state of evidence and future directions*. Apr. 2019. DOI: 10.1111/ane.13062.

[21] Lisa T. Newsome et al. "Coronary Artery Stents: II. Perioperative Considerations and Management". In: *Internatinal Anesthesia Research Society* 107.2 (2008), pp. 570–590.

[22] Albert Chong et al. "Hemodynamic Comparison of Stent-Grafts for the Treatment of Aortoiliac Occlusive Disease". In: *Journal of Endovascular Therapy* 28.4 (Aug. 2021), pp. 623–635. ISSN: 15451550. DOI: 10.1177/15266028211016431.

[23] Yujie Li et al. "A pilot validation of CFD model results against PIV observations of haemodynamics in intracranial aneurysms treated with flow-diverting stents". In: *Journal of Biomechanics* 100 (Feb. 2020). ISSN: 18732380. DOI: 10.1016/j.jbiomech.2019.109590.

[24] Alejandro M. Spiotta et al. "Comparison of techniques for stent assisted coil embolization of aneurysms". In: *Journal of NeuroInterventional Surgery* 4.5 (Sept. 2012), pp. 339–344. ISSN: 17598478. DOI: 10.1136/neurintsurg-2011-010055.

[25] David R. Holmes et al. *Stent Thrombosis*. Oct. 2010. DOI: 10.1016/j.jacc.2010.07.016.

[26] Michael Schuth and Wassili Buerakov. *Particle Image Velocimetry*. 2017. ISBN: 9783319688510. DOI: 10.3139/9783446436619.

[27] Michael Schuth and Wassili Buerakov. "1. Introduction". In: *Particle Image Velocimetry*. 2017, pp. 1–32.

[28] Michael Schuth and Wassili Buerakov. "2. Physical and Technical Background". In: *Particle Image Velocimetry*. 2017, pp. 33–112.

[29] Michael Schuth and Wassili Buerakov. "9. Techniques for 3D-PIV". In: *Particle Image Velocimetry*. 2017, pp. 309–366.

[30] J G Santiago et al. *A particle image velocimetry system for microfluidics*. Tech. rep. 1998, pp. 316–319.

[31] Michael Schuth and Wassili Buerakov. "10. Micro-PIV". In: *Particla Image Velocimetry*. 2017, pp. 367–412.

[32] Nerusupalli Reddy et al. "A study on Refractive index of plasma of blood of patients suffering from Tuberculosis". In: *INTERNATIONAL JOURNAL OF INNOVATIVE TECHNOLOGY AND CREATIVE ENGINEERING* 2.8 (2012), pp. 23–25.

[33] R Budwig. *Refractive index matching methods for*. Tech. rep.

[34] C. Ide and K. Yüksel. "Experimental Investigation of Refractive Index Measurement of Common Solvents and Aqueous Solutions in the Infrared Wavelengths". In: *BALKAN JOURNAL OF ELECTRICAL & COMPUTER ENGINEERING* 6.3 (2018), pp. 159–164.

[35] Wacker Chemie AG. *WACKER*. URL: https://www.wacker.com/h/en-us/silicone-rubber/silicone-gels/wacker-silgel-612-ab/p/000007546.

[36] *Formlabs Community Forum (Index of Refraction)*. URL: https://forum.formlabs.com/t/whats-the-index-of-refraction-of-the-clear-resin/9541.

[37] Linda Kleedorfer. "Method development for the production of flow channels for PIV measurements with the use of additive manufacturing". PhD thesis. Vienna: Institute of Engineering Design and Product Development, 2021.

[38] G Satish et al. *Comparison Of Flow Analysis Of A Sudden And Gradual Change Of Pipe Diameter*. Tech. rep., pp. 2321–7308. URL: http://www.ijret.org.

[39] Vinod Chandavari and Mr Sanjeev Palekar. *DIFFUSER ANGLE CONTROL TO AVOID FLOW SEPARATION*. Tech. rep. 5, pp. 16–21. URL: www.ijtra.com.

[40] S.L. Dixon and C.A. Hall. "Centrifugal Pumps, Fans, and Compressors". In: *Fluid Mechanics and Thermodynamics of Turbomachinery*. Elsevier, 2014, pp. 265–317. DOI: 10.1016/b978-0-12-415954-9.00007-3.

[41] seyyed Mostafa Seyyedi and Rouzbeh Shafaghat. "Design Algorithm of a Free Surface Water Tunnel to Test the Surface-Piercing Propellers (SPP); Case Study Water Tunnel of Babol Noshirvani University of Technology". In: *International Journal of Maritime Technology* 6 (Sept. 2016), pp. 19–30. ISSN: 2345-6000. DOI: 10.18869/acadpub.ijmt.6.19. URL: http://ijmt.ir/article-1-551-en.html.

[42] Nicholas Stanley et al. "A 3-D Printed Optically Clear Rigid Diseased Carotid Bifurcation Arterial Mock Vessel Model for Particle Image Velocimetry Analysis in Pulsatile Flow". In: *ASME Open Journal of Engineering* 2 (Jan. 2023). DOI: 10.1115/1.4056639.

[43] Abdulrazzaq Sulaiman et al. "In vitro non-rigid life-size model of aortic arch aneurysm for endovascular prosthesis assessment". In: *European Journal of Cardio-thoracic Surgery* 33.1 (Jan. 2008), pp. 53–57. ISSN: 10107940. DOI: 10.1016/j.ejcts.2007.10.016.

[44] Tamie L. Poepping, Richard N. Rankin, and David W. Holdsworth. "Flow patterns in carotid bifurcation models using pulsed doppler ultrasound: Effect of concentric vs. eccentric stenosis on turbulence and recirculation". In: *Ultrasound in Medicine and Biology*

36.7 (July 2010), pp. 1125–1134. ISSN: 03015629. DOI: 10.1016/j.ultrasmedbio.2010.02.005.

[45] Helena Sophie Melzer et al. "Numerical simulation and in vitro examination of the flow behaviour within coronary stents". In: *Current Directions in Biomedical Engineering* 5.1 (Sept. 2019), pp. 541–544. ISSN: 23645504. DOI: 10.1515/cdbme-2019-0136.

[46] M G Olsen and R J Adrian. *Out-of-focus effects on particle image visibility and correlation in microscopic particle image velocimetry*. Tech. rep.

[47] Christopher J. Bourdon, Michael G. Olsen, and Allen D. Gorby. "The depth of correlation in micro-PIV for high numerical aperture and immersion objectives". In: *Journal of Fluids Engineering, Transactions of the ASME* 128.4 (July 2006), pp. 883–886. ISSN: 00982202. DOI: 10.1115/1.2201649.

[48] Mark Schult, Christoph Drobek, and Hermann Seitz. "Silicone-based molding technique for optical flow analysis in transparent models of fluidic components". In: *Applied Sciences (Switzerland)* 8.4 (Mar. 2018). ISSN: 20763417. DOI: 10.3390/app8040512.

[49] Majid Y Yousif, David W Holdsworth, and Tamie L Poepping. *Deriving a Blood-Mimicking Fluid for Particle Image Velocimetry in Sylgard-184 Vascular Models*. Tech. rep. 2009.